1971

Laser Excitation Processes In The Cathode Region Of Glow Discharges Through Metal Vapor - Rare Gas Mixtures

Allan Jay Palmer

LASER EXCITATION PROCESSES IN THE CATHODE REGION OF GLOW DISCHARGES THROUGH METAL VAPOR - RARE GAS MIXTURES

by

Allan Jay Palmer

Department of Physics

Submitted in Partial Fulfillment
of the requirements for the degree of

Doctor of Philosophy

Faculty of Graduate Studies
The University of Western Ontario
London, Canada

January 1971

ABSTRACT

The limitations to achieving higher power and efficiency in metal vapor - rare gas lasers operating in the positive column of a discharge are discussed on the basis of the Shottky model of the positive column. Detailed calculations are carried out which quantitatively interpret the quenching behavior which occurs in the He-Zn positive column laser with increasing Zinc concentration.

The suitability of the cathode region to overcome the limitations on maximum discharge current and metal vapor concentration in metal vapor - rare gas lasers is discussed. An experimental investigation of the spectral characteristics of the cathode region is undertaken which reveals the occurrence of quenching behavior similar to that of the positive column, and the existence of anomalously shaped profiles of the spontaneous emission intensity from charge-transfer excited lines in He-Zn across the cathode region. A theoretical model analogous to the Shottky model is developed which allows qualitative interpretation of these observations. The model is used to set criteria for optimizing the design of future cathode region - lasers.

Observations on a triode discharge through a Helium-Cadmium mixture are reported which show that a negatively biased grid in

the vicinity of the negative glow effects a dramatic enhancement of the efficiency for exciting the laser lines in the negative glow region of the discharge. Possible applications of the effect are discussed.

Finally, a computer program using the Bates-Damgaard approximation of oscillator strengths is developed which predicts population inversions and practical negative absorbtion coefficients for several transitions of MgII resulting from accidentlly resonant charge-transfer collisions and cascade processes in the Ne-Mg system.

ACKNOWLEDGEMENTS

The author wishes to express his sincere thanks to Professor J. Wm. McGowan for his encouragement of this work and for many helpfull discussions.

TABLE OF CONTENTS

page

LIST OF TABLES

LIST OF FIGURES

CHAPTER I

INTRODUCTION

Suggestions made over the past five years[1-4] that accidentally resonant charge-transfer collisions could be effective in generating population inversions have recently been confirmed by Jensen, Collins, and Bennet[5] in their afterglow studies on the He-Zn laser. Their evidence indicates that laser excitation of the Zinc ion results from reactions of the type:*

$$He^+ + Zn \rightarrow (Zn^+)^* + He \qquad 1$$

and

$$He_2^+ + Zn \rightarrow (Zn^+)^* + 2He \qquad 2$$

Also, the proximity of the upper laser level energy to the rare gas ionization potential in several other metal-vapor-rare-gas lasers investigated by Silvfast[7] leads one to suspect that charge-transfer plays an important role in

---

*In a more recent report by Collins,[6] Penning reactions are estimated to be dominant over reaction #2.

many of these systems.

This mechanism has an important consequence to gas laser technology, namely, it provides for the first time carriers of resonant excitation with charge. The possibility of interacting electric and magnetic fields with these carriers seems to open up a new degree of freedom in the design of gas lasers. We will be considering the important example of the possible use of the strong electric fields which exist in the cathode region of a glow discharge.

It is not surprising that, in the ten years since the development of the first gas-discharge laser by Javan, the positive column region of the discharge has enjoyed almost exclusive application to practically all gas laser systems including the metal vapor - rare gas lasers. The properties of the positive column make it a region which suits naturally the basic requirements of laser design. It is the one region of the discharge which can be stretched to any length between the electrodes, and can be confined to a large range of diameters to provide a correspondingly large range of current densities. Also it has, relative to other possible lasing regions, a low ratio of average electric field to active volume necessary for optimal overall efficiency. However, there are fundamental limitations which

attend the use of the positive column for many gas laser systems, and the metal vapor - rare gas systems are notable examples.

The plots by Jensen, et al.[5] of the c.w. output power from the He-Zn laser vs. tube temperature and discharge current reveal the two basic limitations of a positive column charge-transfer laser. Consider first the limitation on the maximum concentration of Zn vapor (tube temperature). This limitation is well understood and is due to the familiar fact that the electron temperature in the positive column of a rare gas - metal vapor mixture falls suddenly with an increase in the relative concentration of the metal vapor above about 0.1%.[8] This causes a corresponding drop in production rate of rare gas ions which are being used to excite the upper laser levels, and eventually extinguishes the laser action. Thus for a fixed discharge current, the laser output reaches a maximum at a certain optimal value of the tube temperature which, for the He-Zn system, corresponds to a relative concentration of Zn of only about 0.1%. Secondly, at fixed tube temperature there is an optimal discharge current which, when exceeded, causes the output (from the two transitions excited by reaction #2) to fall quite rapidly. This results, most

likely, from radiation trapping on transitions between the lower laser levels and the ZnII ground state.

Thus, there are at least two requirements which must be met in order more fully to exploit charge transfer as an effective laser excitation mechanism. First, average electron energies must be made high enough so that the production rate of the excitation carrier ions is not sensitive to the relative concentration of the lower ionization potential component in the mixture. Second, the metal vapor ions must be removed at a faster rate in order to abate the radiation trapping.

The Crookes dark space of a glow discharge (see Figure III-1) seems, at first, to satisfy both of these requirements automatically. In pure gasses the ions which enter the Crookes dark space are produced by electron collisions in the negative glow. The strong electric fields which exist in the dark space impart to the so-called primary group of electrons which enter the negative glow an average energy which is large compared with the ionization potential of either a metal vapor or a rare gas. Thus the production of excitation carrier ions by these electrons will be insensitive to the relative concentration of a metal vapor component. This argument makes the negative glow itself a region of

interest for obtaining laser action in metal vapor - rare gas mixtures. This fact, together with the possibility of deriving the metal vapor through sputtering, has evidently motivated the recent construction of several hollow cathode, metal vapor - rare gas lasers[6,9-11].

We have also, in the Crookes dark space, the required enhancement of the rate of removal of ground state Zn ions. Under typical operating conditions (see Chapter III), the width of the dark space will be comparable to the diameter of the positive column laser. However, ion velocities in the dark space will be close to two orders of magnitude larger than the ambipolar diffusion velocity of the ions in the positive column. This in itself permits potentially two orders of magnitude higher power operation in the dark space.

On the basis of the above picture of the cathode region, a tentative model of a charge-transfer excited laser operating in the Crookes dark space was proposed and calculations were performed for the He-Zn system which indicated that laser action should be achievable in the dark space over a fairly wide range of cathode fall parameters and suggested a possible enhancement of the output power density over that from a positive column laser by a factor of

the order of $10^1 - 10^2$.[12] (See Section III.2, below.)

Relevant studies of the spectral and electrical properties of the cathode region in glow discharges through metal vapor - rare gas mixtures which thus appeared might have considerable value to gas laser technology were found to be virtually nonexistent. A primary aim of this thesis is therefore to carry out experimental and theoretical studies sufficient to formulate a model of excitation processes occurring in the cathode region of a glow discharge through a metal vapor - rare gas mixture which may be used to evaluate more confidently the suitability of the cathode region as an environment for exciting laser action in these systems.

We begin our study in Chapter II by reviewing the Shottky theory of the positive column. We use the theory to calculate the dependence on relative Zn concentration of the intensity of a charge-transfer excited laser line in the positive column of a He-Zn discharge. Our results compare well with the characteristics reported by Jensen, et al.[5] for their He-Zn laser.

In Chapter III, we first review the theory of the abnormal cathode fall in pure gasses. We then present the preliminary model of a charge-transfer excited laser

operating in the Crookes dark space. The results of our spectroscopic studies of the cathode region in He-Zn and He-Cd discharges are presented next. These results show the need for considerable modification of the preliminary model. A more complete model is then formulated which is capable of qualitative interpretation of the results.

Chapter IV presents spectral observations on the cathode region of a triode discharge through the He-Zn and He-Cd systems. We report a dramatic and unexpected enhancement of the efficiencies for exciting the laser transitions in the negative glow when the grid of the triode is biased negatively (with respect to the plasma) in the vicinity of the negative glow. Interpretation and applications of the effect are discussed.

Complementary to our studies of the discharge excitation processes, we present in Chapter V computer calculations of MgII level populations expected to arise from accidentally resonant charge-transfer excitation and cascades in a Ne-Mg system. Several inversions are found which, assuming reasonable values for the charge-transfer cross-sections, have practical gains.

In Chapter VI we draw some general conclusions on the basis of the new information contributed in Chapters III-V,

and point to relevant future studies and applications.

CHAPTER II

EXCITATION PROCESSES IN THE POSITIVE COLUMN

One of the primary aims of this thesis is to develop a model of the cathode region of a glow discharge analogous to the Shottky diffusion model of the positive column which will be applicable to an analysis of laser excitation in the cathode region. We therefore devote this chapter to a review of the Shottky theory and to an application of the theory to a metal vapor - rare gas laser operating in the positive column.

In section one we review briefly the Shottky theory of the positive column in pure gasses. In section two we discuss the adaptation of this model to the positive column of a discharge through a metal vapor mixture, and in section three we apply the theory to the He-Zn laser and compare the results of the calculations with the operating characteristics reported by Jensen, et al.[5] for their He-Zn laser.

II-1: Review of the Shottky Theory

This treatment regards the electron temperature, T_e, the longitudinal field, X, and the ion concentration, N_+ as the basic unknowns and starts with the following simplifying assumptions:

1. The electron energy distribution is Maxwellian.
2. The electron temperature is constant across the discharge.
3. The column is electrically neutral.

The basic equation underlying the theory is simply the steady-state rate equation for the ion concentration:

$$dN_+/dt = Z(P,T_e) - f(P,r_o,T_e) = 0 \qquad \text{(II-1)}$$

where $Z(P,T_e)$ is the ionization rate per unit volume, and $f(P,r_o,T_e)$ is the rate of loss of ions per unit volume. P, T_e, and r_o are the pressure, electron temperature, and tube radius, respectively. In the Shottky theory one assumes the loss rate is due entirely to ambipolar diffusion of the ions to the walls. For the cylindrically symmetric case, eq.(II-1) then takes the form:

$$d^2N_+/dr^2 + (1/r)\, dN_+/dr + (Z/D_a)\, N_+ = 0 \qquad \text{(II-2)}$$

where D_a is the ambipolar diffusion constant for the ions. The relevant solution is:

$$N_+(r) = N_+(0)J_o(r\sqrt{Z/D_a}) \qquad \text{(II-3)}$$

where J_o is the zeroth order Bessel function. The boundary condition, $N_+(r_o) = 0$, is then imposed to obtain,

$$r_o\sqrt{Z/D_a} = 2.4. \qquad \text{(II-4)}$$

D_a is given to good approximation by [13],

$$D_a = (kT_e/e)k_+ \qquad \text{(II-5)}$$

where k is Boltzman's constant, e is the electronic charge, and k_+ is the ion mobility. Z is calculated by integrating over a Maxwell distribution a standard assumed form for the ionization cross section which grows linearly with energy from zero at threshold.[8] The result is:

$$Z = aP(m_e/e)(4/\sqrt{\pi})(2kT_e/m_e)^{3/2}(1 + \tfrac{1}{2}\tfrac{eV_i}{kT_e})\exp(-eV_i/kT_e) \qquad \text{--- (II-6)}$$

where m_e is the electron mass, a is the initial slope of the ionization cross section as a function of energy, and V_i is the ionization potential of the gas. Inserting into equation (II-4), the above expressions for D_a and Z, reduces finally, for $eV_i/kT_e \gg 1$, to:

$$(1/\sqrt{eV_i/kT_e})\exp(eV_i/kT_e) = 1.16X10^7C^2P^2r_o^2 \qquad \text{(II-7)}$$

with

$$C^2 = aV_i/(k_+P) \qquad \text{(II-8)}$$

This well known relation allows one to plot T_e/V_i against (CPr_o) giving a universal curve for all gasses. The curve

is reproduced in most references on gas discharges.[13]

The remaining unknown, X, follows from conservation of energy. The average energy gained by an electron from the field is simply balanced against the energy lost by collisions. The end result is[13]

$$eX = \frac{3}{\sqrt{2}} k^{1/2} (kT_e/\lambda_e) \qquad \text{(II-9)}$$

where k is the fractional energy lost per collision and λ_e is the electron mean free path.

Deviations of the theory from experiment in pure gasses are due in most cases to various nonlinear phenomena such as step-wise excitations, gas heating, etc. For a more detailed discussion of the limitations of the theory see ref.(8).

II-2: Extension of the Theory to Metal Vapor - Rare Gas Mixtures

It has long been known that the addition of very small quantities of metal vapor to a rare gas discharge can have pronounced effects on the electrical and spectral properties of the positive column. It has also been generally recognized that the effects at very low percentage concentration within the approximate range, 10^{-4} - 10^{-2} % are mostly attributable to inelastic collision processes of the

metal vapor atoms with rare gas metastables. Beyond this range the metastables have usually been used up, resulting in a saturation of the effects with further increase in the metal vapor concentration. The observed rapid drop of the electron temperature with increasing metal vapor concentration in the range 10^{-2} - 1 % can be attributed to direct electron collisional ionization of the metal vapor. It is in this range that the existing metal vapor - rare gas lasers operate, and in this case the obvious generalization of the Shottky theory is obtained by replacing eq.(II-2) with:[8]

$$\frac{kT_e}{e}\left[\frac{d^2N_e}{dr^2} + \frac{1}{r}\frac{dN_e}{dr}\right] + \left[\frac{Z_1}{k_{+1}} + \frac{Z_2}{k_{+2}}\right]N_e = 0 \qquad \text{(II-10)}$$

which has a solution, analogous to eq.(II-4), of the form,

$$\frac{Z_1}{k_{+1}} + \frac{Z_2}{k_{+2}} = \frac{kT_e}{e}\left(\frac{2.4}{r_0}\right) \qquad \text{(II-11)}$$

The subscripts label the ionization coefficients and mobility of the two components in the mixture.

II-3: Application of the Theory to the He-Zn Laser

The quenching action that occurs in the metal vapor - rare gas lasers as the metal vapor is increased has thus far been given only qualitative interpretation on the basis

of the known drop in the electron temperature as metal vapor is introduced into rare gas discharges.[6] A quantitative comparison of the quenching predicted by eq.(II-11) with the corresponding behavior occurring in the metal vapor - rare gas lasers has not yet appeared in the literature. To illustrate the ability of this model to predict with reasonable accuracy the quenching action in these lasers, we have used equation (II-11) to calculate the relative intensity of a charge-transfer excited line in the He-Zn system as a function of the relative Zn concentration in the mixture.

Using eq.(II-6) for the ionization coefficients, eq.(II-11) may be written in the form:

$$R'A + B = 4.2 \cdot 10^{-8} (C_2 \cdot r_0 \cdot P)^{-2} \cdot (V_2/T_e)^{1/2} \qquad \text{(II-12)}$$

Here,

$$A = \left[1 + \tfrac{1}{2} \frac{V_1}{T_e}\right] e^{-V_1/T_e} \qquad \text{(II-13)}$$

$$B = \left[1 + \tfrac{1}{2} \frac{V_2}{T_e}\right] e^{-V_2/T_e} \qquad \text{(II-14)}$$

$$R' = \left(\frac{C_1'^2}{C_2^2}\right) \cdot R \qquad \text{(II-15)}$$

The subscripts 1 and 2 refer to the Zinc and Helium components, respectively. C_2 is defined by eq.(II-8). C_1 is

also defined by eq.(II-8) except that the mobility is that of the Zinc ion in Helium, and the pressure refers to the Helium pressure. R is the relative concentration of Zinc to Helium.

At constant current, the intensity of a ZnII line which is excited by Helium ions through charge-transfer is, to a good approximation, proportional to the product (R'B). (Over a practical range of interest we can neglect both the temperature dependence of the ion loss rate and the $T_e^{3/2}$ dependence in Z_2 relative to the exponential dependence on T_e).

Eq.(II-12) must first be solved for T_e as a function of R', and then the product (R'B) may be plotted as a function of R'. The ratio, C_1^2/C_2^2 can then be used to scale R' to R, and one can then compare the calculated results with the observed dependence of the intensity of a charge-transfer excited line on R, reported by Jensen, et al. [5] for the He-Zn laser.

Using the values, r_o = 0.2 cm, and P = 6 Torr which were used by Jensen, et al.[5], and taking $C_2 = 3.9\text{X}10^{-3}$ from tables [13], eq.(II-12) becomes:

$$R'A + B = 1.83\text{X}10^{-3}(V_2/T_e)^{\frac{1}{2}} \qquad \text{(II-16)}$$

Substituting V_1 = 9.39 eV, and V_2 = 24.48 eV for the Zinc and

Helium ionization potentials, we have solved eq.(II-16) graphically for T_e as a function of R', and $R' \cdot B$ as a function of R'. The graphs appropriate to these calculations are presented in Figures II-1 - II-3.

The parameter, C_1 needed to scale R' to R has not been tabulated as has C_2. We have therefore used mobility and ionization data obtained from ref.(14) and estimated C_1 $1.5 \cdot 10^{-2}$. Figure II-4 shows the comparison of the calculated and observed dependence of the charge-transfer excited emission on R. The agreement must be regarded as good, considering our neglect of the various nonlinear processes.

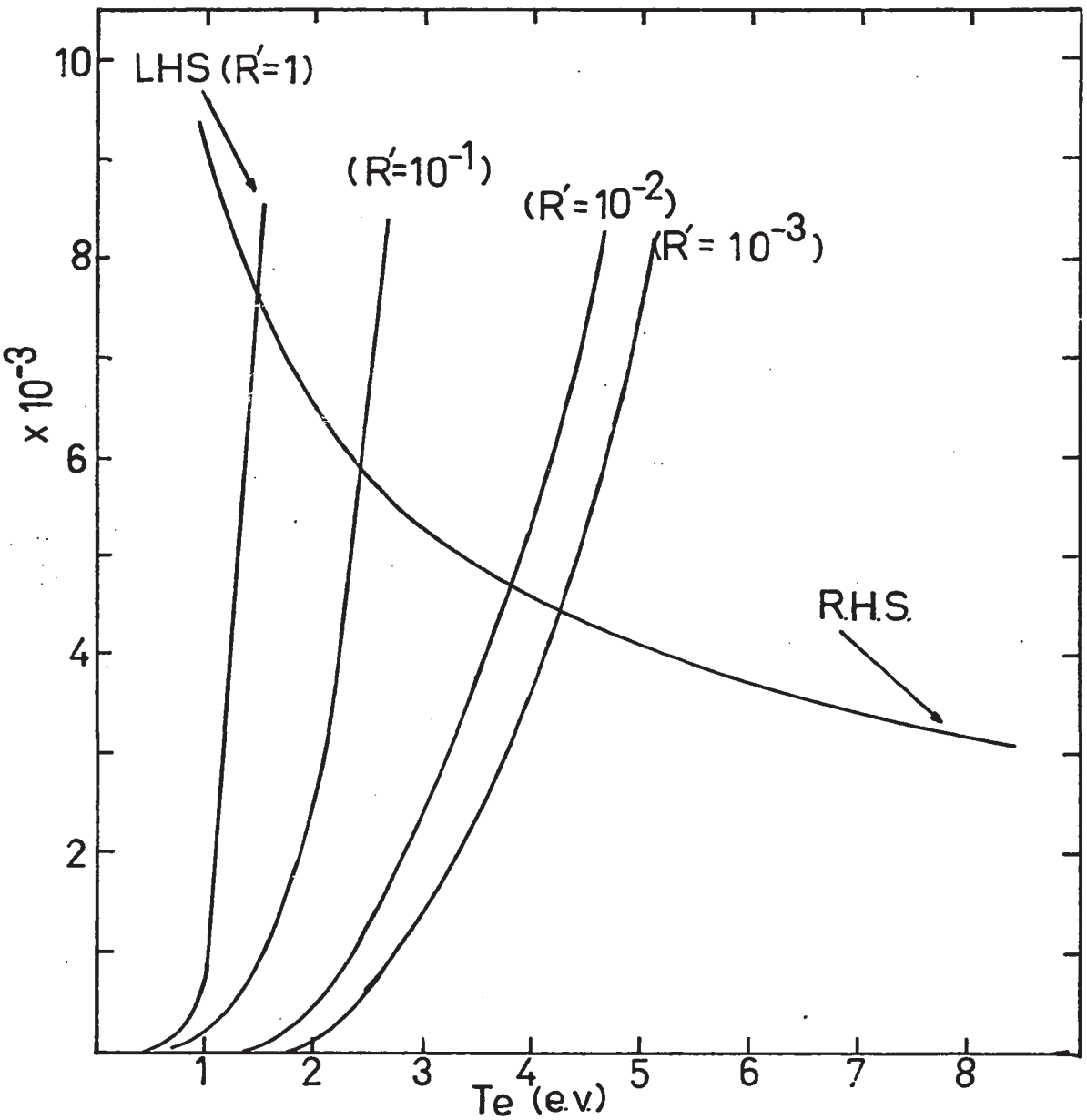

Fig (II-1)

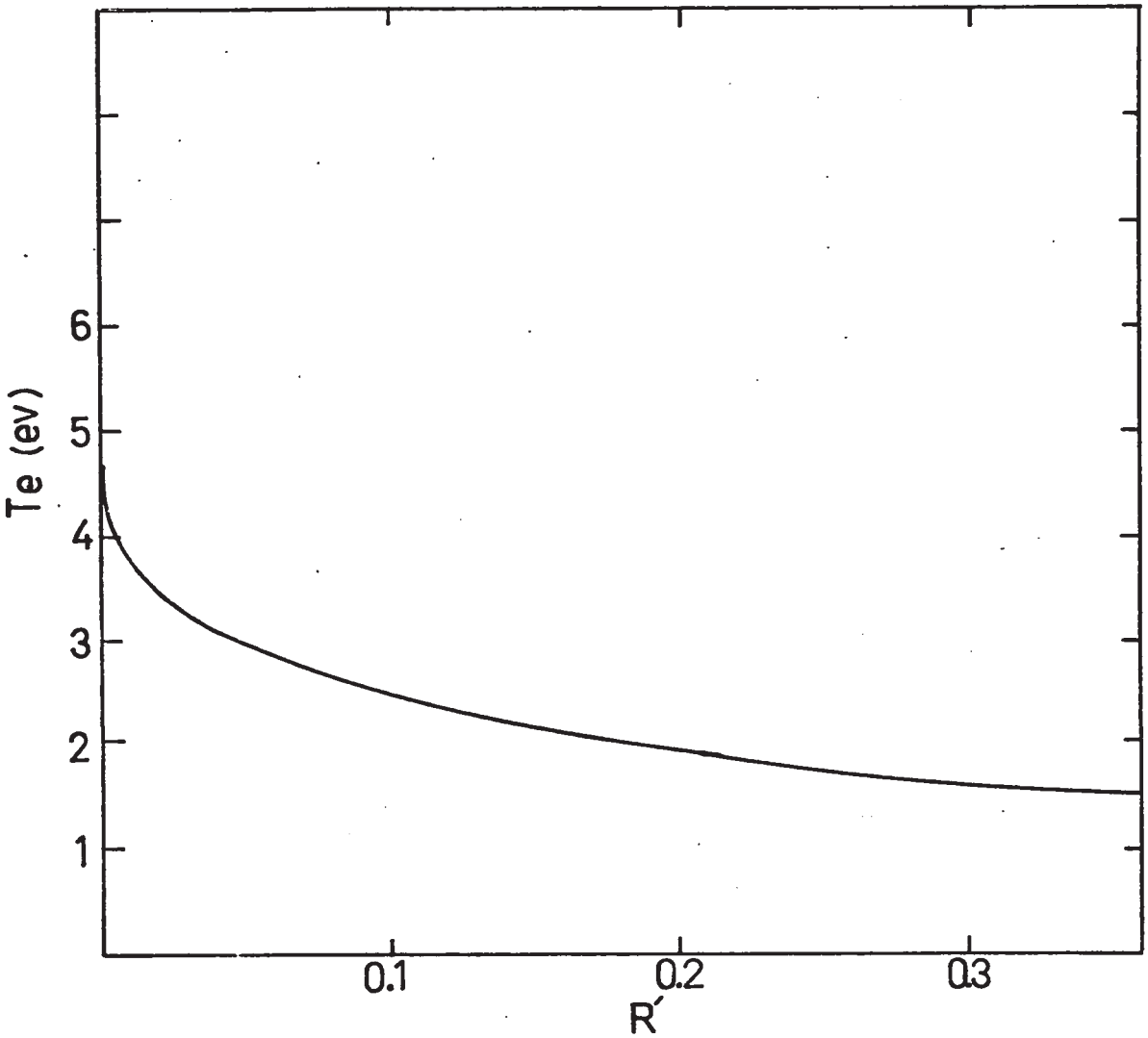

Fig (II-2)

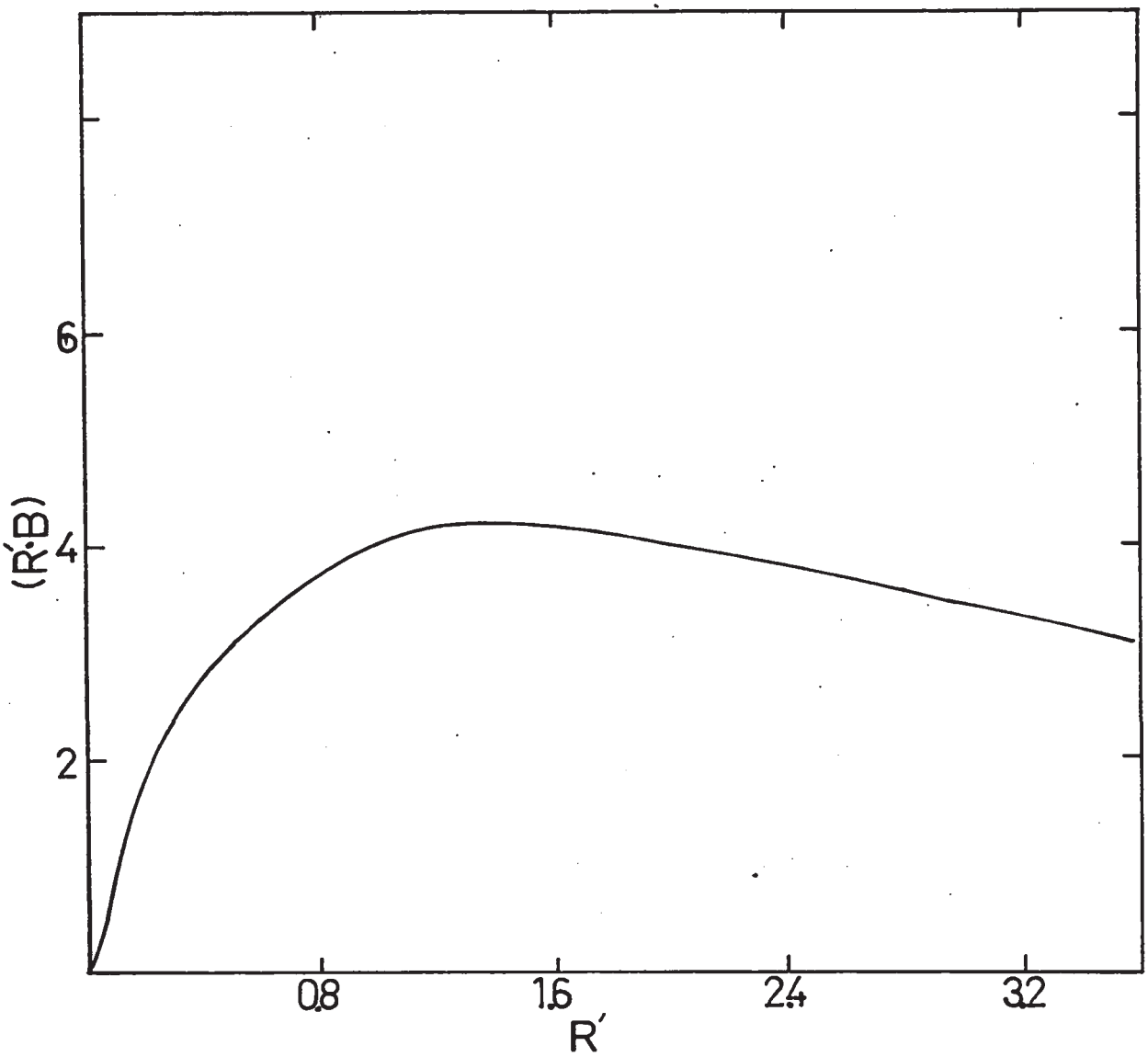

Fig (II-3)

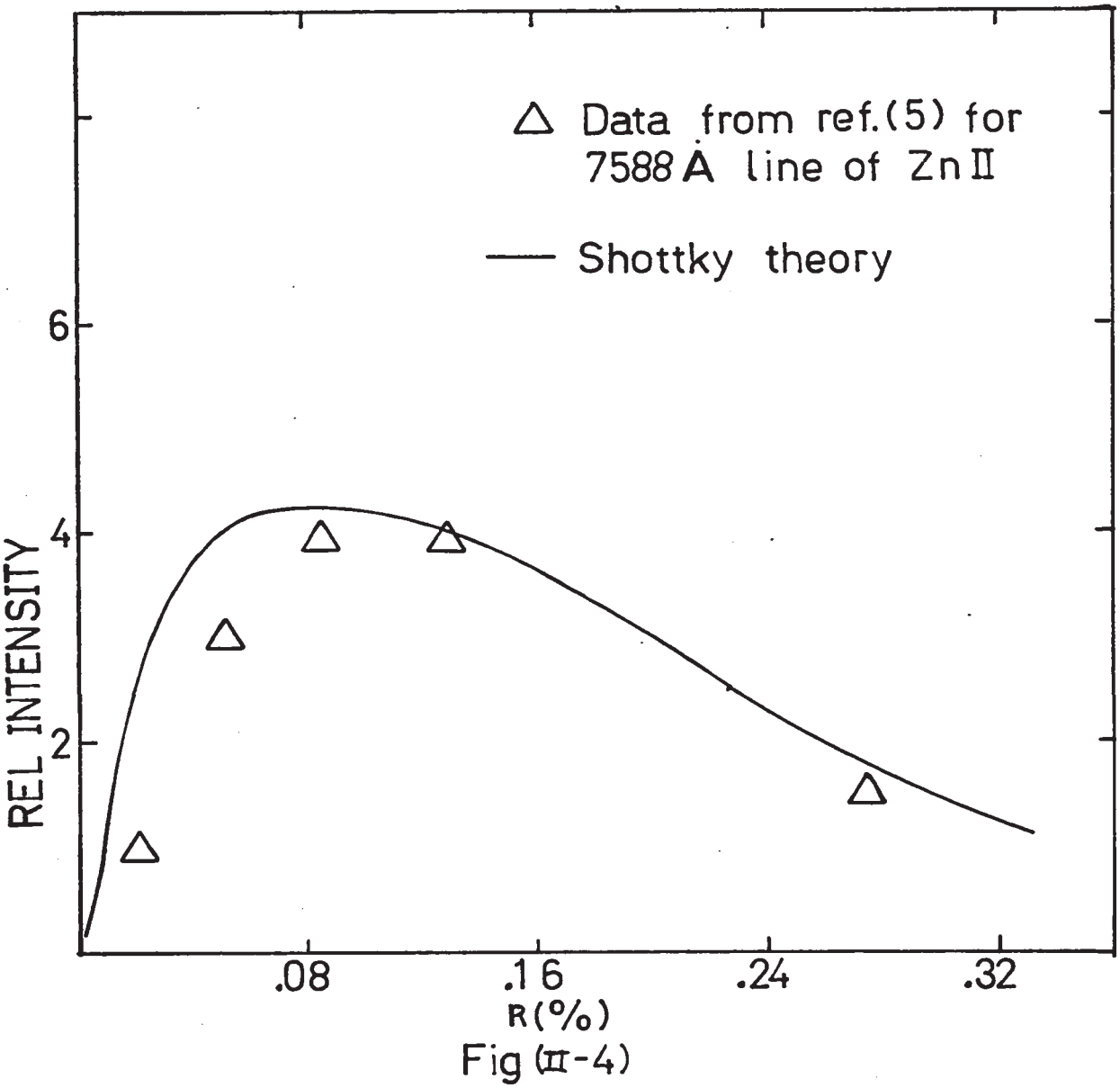
△ Data from ref.(5) for
7588 Å line of Zn II
—— Shottky theory
REL INTENSITY
6
4
2
.08
.16
.24
.32
R(%)

Fig (II-4)

CHAPTER III

EXCITATION PROCESSES IN THE CATHODE REGION

We turn our attention now to the cathode region of a glow discharge. We define this region as the region which lies between the cathode and the Faraday dark space as indicated in Figure III-1. It contains, in order of their appearance from the cathode, the aston dark layer, cathode glow, Crookes dark space, and the negative glow. Unlike the positive column which is close to being electrically neutral, the cathode region contains strong positive space charge, and this gives rise to the high electric fields in the Crookes dark space which, as referred to in the introduction, may benefit this region as an environment for charge-transfer excited laser action.

It is well known that the cathode region is, electrically, the most important part of the discharge. Here is where processes essential to the maintenance of the discharge take place. The fundamental processes which occur in the cathode region are the following: 1) Electrons emitted from the cathode are accelerated across the dark

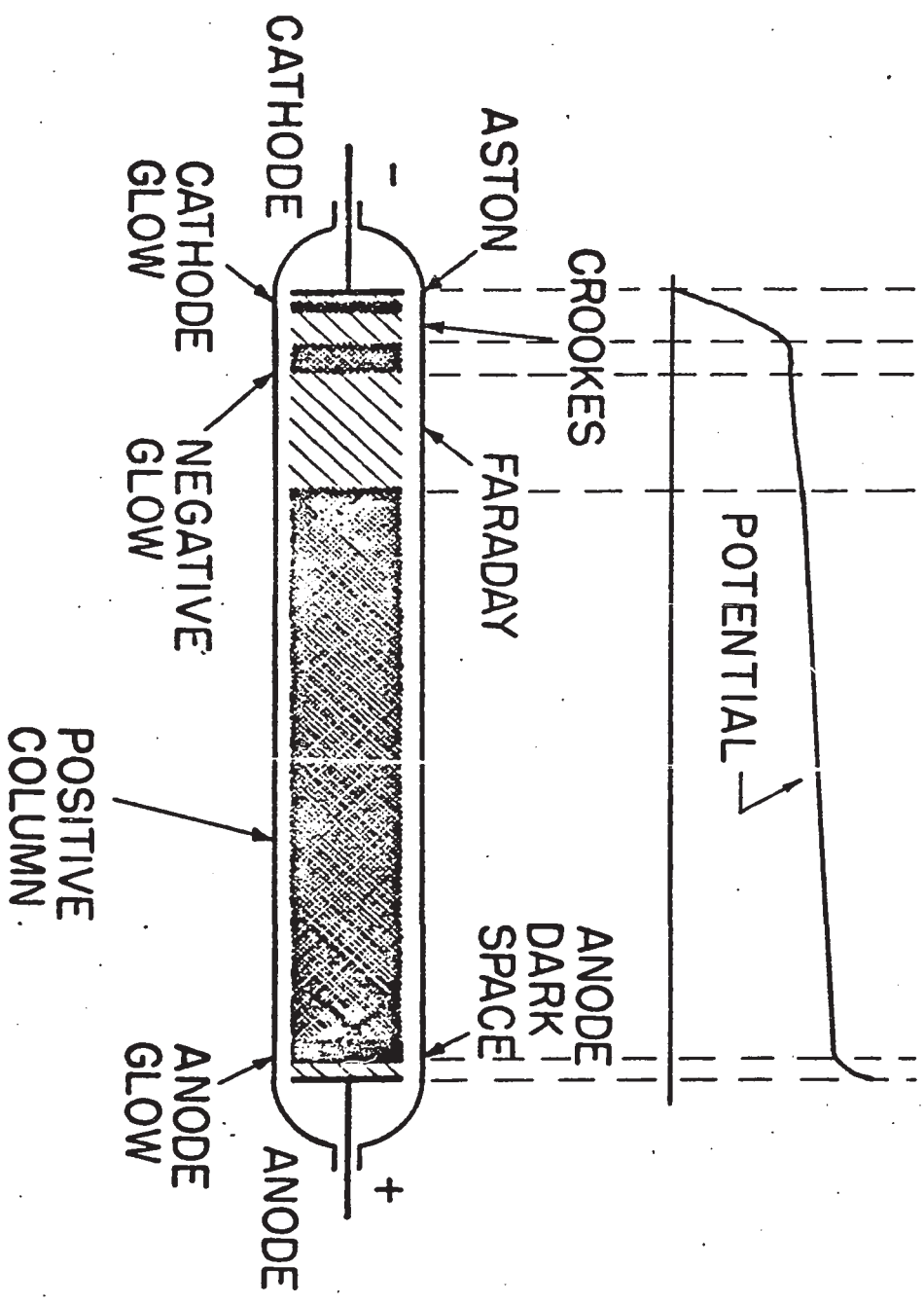
CATHODE
ASTON
CROOKES
FARADAY
POTENTIAL
CATHODE GLOW
NEGATIVE GLOW
POSITIVE COLUMN
ANODE DARK SPACE
ANODE GLOW
ANODE
-
+

FIG. III-1

region, excite and ionize the gas, and are multiplied by a factor M; 2) positive ions, excited and neutral molecules, and photons hit the cathode and release new electrons. If we define an efficiency, γ , as the number of electrons released from the cathode per electron formed in the multiplication process, we have the well known conditions for maintenance of the discharge:

$$\gamma (M - 1) = 1 \qquad \text{(III-1)}$$

which states simply that an electron emitted from the cathode must produce sufficient ionization and excitation to cause the emission of one other electron from the cathode.

III.1: SIMPLE THEORY OF THE CATHODE FALL

In this section, we sketch briefly a simple theory of the cathode fall due to Little and Von Engle[13] which is based on the above maintenance condition and some simplifying assumptions. The object of the theory is to obtain relations between the potential drop across the dark space, V_c, the current density, j, and the thickness of the dark space, d.

The following assumptions are made in the theory:

1. A linear variation of the field in the Crookes dark space, which most measurements indicate, is assumed.
2. Due mainly to the higher speeds of the electrons, electron space charge in the dark space is neglected.
3. The ion velocity in the dark space is assumed to be governed by symmetric charge-transfer.
4. The electrons ejected from the cathode are assumed to belong to two groups: electrons released by ions from the Crookes dark space, and electrons released by photons from the negative glow.

Using Poison's equation to relate the field to the ion space-charge together with the above assumptions, an equation is derived of the form:

$$i/P^2 = C \frac{V_c^{3/2}}{(P \cdot d)^{5/2}} \qquad \text{(III-2)}$$

and where P is the pressure, C contains various constants characteristic of the gas and cathode surface, and also a voltage-dependent efficiency factor for the photoejection of secondary electrons.

The theory then assumes that the electron multiplica-

tion can be described as:

$$j_{e_G} = j_{e_K} \exp(\bar{\eta}_i V_c) \qquad \text{(III-3)}$$

where j_{e_G} and j_{e_K} are the electron current densities at the negative glow boundary and cathode, respectively. $\bar{\eta}_i$ is taken as the average ionization coefficient in the cathode fall. This relation, substituted into the maintenance equation (III-1), gives:

$$\bar{\eta}_i V_c = \log\left[\frac{1+\gamma_p}{G+\gamma_p}\right] \qquad \text{(III-4)}$$

where γ_p and G are, respectively, the ion and photon efficiencies for electron emission from the cathode.

Equations (III-2) and (III-4) are the principal results of the theory. With $\bar{\eta}_i$ regarded as a given function of the reduced field, it is possible to obtain $j/p^2 = f_1(V_c)$ and $V_c = f_2(p \cdot d)$. The results also enable one to explain the existence of the so-called normal and abnormal cathode falls on the basis of a minimum occurring in the functions $V_c = f_2(p \cdot d)$ and $V_c = f_1^{-1}(j/p^2)$. The theory is in reasonable agreement with experiment for most gasses.

III.2: PRELIMINARY MODEL OF A CHARGE-TRANSFER EXCITED LASER OPERATING IN THE CROOKES DARK SPACE[12]

The apparent suitability of the cathode region as an environment for charge-transfer excited laser action has been discussed in the introduction. Let us now proceed to make a preliminary order of magnitude estimate of the cathode fall parameters required to obtain laser action from the He-Zn system in the Crookes dark space.

Threshold requirements may be estimated from the discharge parameters reported in Ref.(5) for the positive column laser. The electron temperature at optimal Zinc concentration has already been calculated in Chapter II. We also know that at the reported He pressure of 4 Torr, molecular Helium ions are produced via the Hornbeck-Molnar process[15] at about the same rate as the He ions. This information allows us to estimate the relative concentration of the three major ion species. We find, in order of magnitude, $n_{He^+} \sim n_{He_2^+} \sim n_{Zn^+}$. The electric field and hence the electron drift velocity is also related to the electron temperature (see eq.(II-9)). Using a plot of eq.(II-9) from Ref.(13) and electron mobility data from Ref.(14), we calculate $V_e(\text{drift}) \sim 10^6 \text{cm/sec}$. Charge neutrality then gives the ion concentration:

$$3n_{He^+} \sim n_e \sim j/(e \cdot V_e(\text{drift})) \qquad \text{(III-5)}$$

or

$$n_{He^+} \sim 10^{12}\ cm^{-3} \qquad \text{(III-6)}$$

using the reported threshold current density. The threshold product of Zn concentration with the effective ion flux, ϕ_i, is then:

$$\phi_i n_{Zn} = n_i (3M_i kT_{gas})^{\frac{1}{2}} n_{Zn} \approx 10^{31} cm^{-5} sec^{-1} \qquad \text{(III-7)}$$

where M_i and T_{gas} are the ion mass and gas temperature respectively.

In the Crookes dark space the discharge current is carried mainly by the ions. We will assume further, on the basis of the argument already presented in the introduction, that these ions will be predominantly Helium ions over a much larger range of Zinc partial pressure than is the case in the positive column. (This assumption will be judged more carefully in the last sections of this chapter.) Within the pressure range of interest (1-10 Torr) we can assume again approximately equal rates of production of molecular and atomic Helium ions. With these assumptions, the threshold condition for charge-transfer laser action in the Crookes dark space becomes:

$$j \cdot n_{Zn} \sim 2 j_i \cdot n_{Zn} \sim 3 \phi_i \cdot e \cdot n_{Zn} \sim 10^{12} (amp/cm^2)\, cm^{-3} \qquad \text{(III-8)}$$

Now, as in the positive column laser, the current density and metal vapor concentration in such a "cathode"

laser will be limited, but for fundamentally different reasons. The limitation on the current density is due to the fact that the width of the dark space decreases with increasing current density. The metal vapor concentration will ultimately be limited due to the decrease in ionic mean free path for asymmetric charge-transfer to a distance shorter than the width of the dark space.

In the absence of saturation or other nonlinear processes, the total laser output power from the Crookes dark space should vary as:

$$P \propto j \cdot d \cdot n_{Zn} \qquad \text{(III-9)}$$

where d is the width of the dark space which depends on j, and the optimal Zinc concentration would be given by:

$$\ell_{ct} \equiv (\sigma_{ct} \cdot n_{Zn})^{-1} = d \qquad \text{(III-10)}$$

where σ_{ct} and ℓ_{ct} are the cross section and corresponding mean free path for asymmetric charge-transfer of the Helium ions on Zinc. In this case eq.(III-9) becomes:

$$P \propto j \qquad \text{(III-11)}$$

In their afterglow studies Jensen, et al.[5] estimate $\sigma_{ct} \sim 4 \cdot 10^{-15}\ cm^2$. Using this value in eq.(III-10) and

combining with eq.(III-8), the threshold condition becomes:

$$j/d \sim 2\cdot 10^{-3} (amp/cm^2)\cdot cm^{-1} \qquad \text{(III-12)}$$

Figure III-2 shows this condition superimposed onto the abnormal cathode fall characteristics for pure He. (It is consistent to assume that if the production of Helium ions in the negative glow is insensitive to the metal vapor concentration then the electrical behavior of cathode region should also be relatively insensitive to the metal vapor concentration.)

It is obvious that there will be a minimum value for d below which diffraction losses will extinguish the laser action. If we estimate this value for d to be roughly 1 mm, we see from the plot that laser action should be achievable over a fairly wide range of cathode fall parameters.

We can also judge, by comparing the plot with the reported characteristics of the positive column laser, that if saturation or other nonlinear processes do not occur then the maximum output from a 1 cm wide He-Zn laser of this type should be between one and two orders of magnitude stronger than that from a positive column laser of the same active volume. Also, there is nothing to prohibit using a substantially greater cathode surface area to gain more

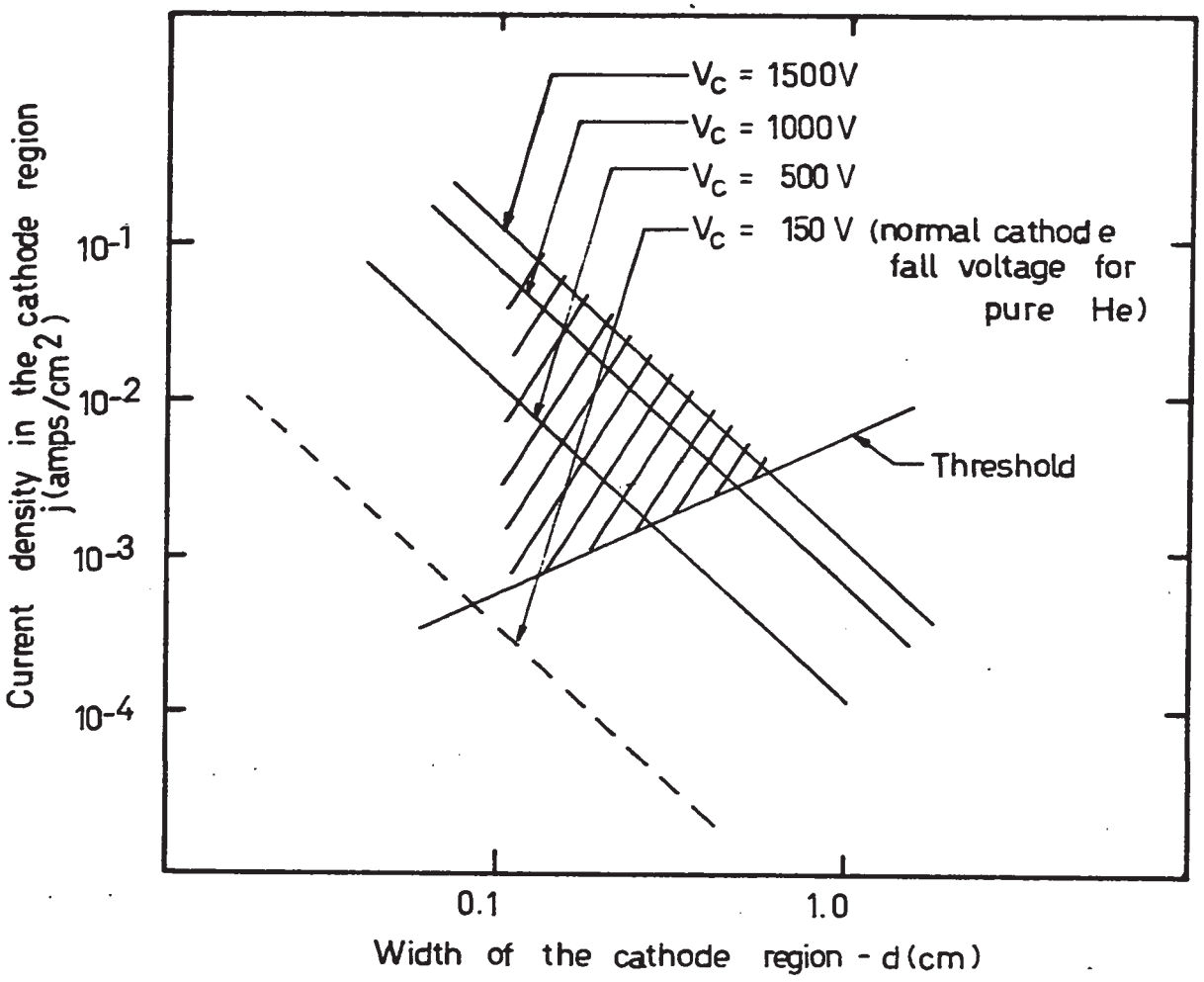
V_c = 1500V
V_c = 1000V
V_c = 500 V
V_c = 150 V (normal cathode fall voltage for pure He)
Threshold
Current density in the cathode region j(amps/cm^2)
10^{-1}
10^{-2}
10^{-3}
10^{-4}
0.1
1.0
Width of the cathode region - d(cm)

Fig. (III-2)

power. The overall efficiency, E, of such a laser would be low ($E \propto 1/V_c$ from eq.(III-11)). This is due to the large amount, relative to the active volume of the laser, of cathode surface area and negative glow volume, in which a large fraction of the discharge energy is dissipated. It can also be anticipated that there might appear in the Crookes dark space other laser transitions in many systems which, due to bottleneck processes or competing electron collisional excitations, cannot be inverted in the positive column.

In the absence of previous work on the spectral and electrical properties of the cathode region in glow discharges through metal vapor rare gas mixtures, we have made, in the above model, some rather essential assumptions regarding the ionization processes. Specifically, we have assumed, within the range of application of the model, that the production rate of rare gas ions remains insensitive to the metal vapor concentration and that these ions form the dominant contribution to the ion current in the Crookes dark space. The very attractive possibilities derived from these assumptions warrant a thorough investigation of them. The remainder of this chapter reports the results of such investigations.

III.3: EXPERIMENTAL PROCEDURE

The principal aims of the experimental studies to be described in this section are threefold:

1. To observe the dependence of spectral intensities and the electrical characteristics of the cathode region on the relative concentration of metal vapor in discharges through He-Zn and He-Cd mixtures.
2. To make observations on the profiles of the spontaneous emission intensities from these mixtures across the cathode region.
3. To attempt to observe c.w. laser action in the cathode region in the He-Zn and He-Cd systems.

A partial energy level diagram relevant to the He-Zn and He-Cd systems is shown in Figure III-3.

III.3-1: The Discharge Tube

The electrode configuration within the discharge tube consisted of three 25cm X 0.5cm X 0.3cm rectangular cathodes placed end to end and aligned parallel to the optic axis of the discharge tube. Each cathode had an associated anode of approximately the same dimensions placed directly across from the cathode at a distance of 1.5cm. The arrangement is shown schematically in Figure III-4. This arrangement was chosen over a hollow cathode

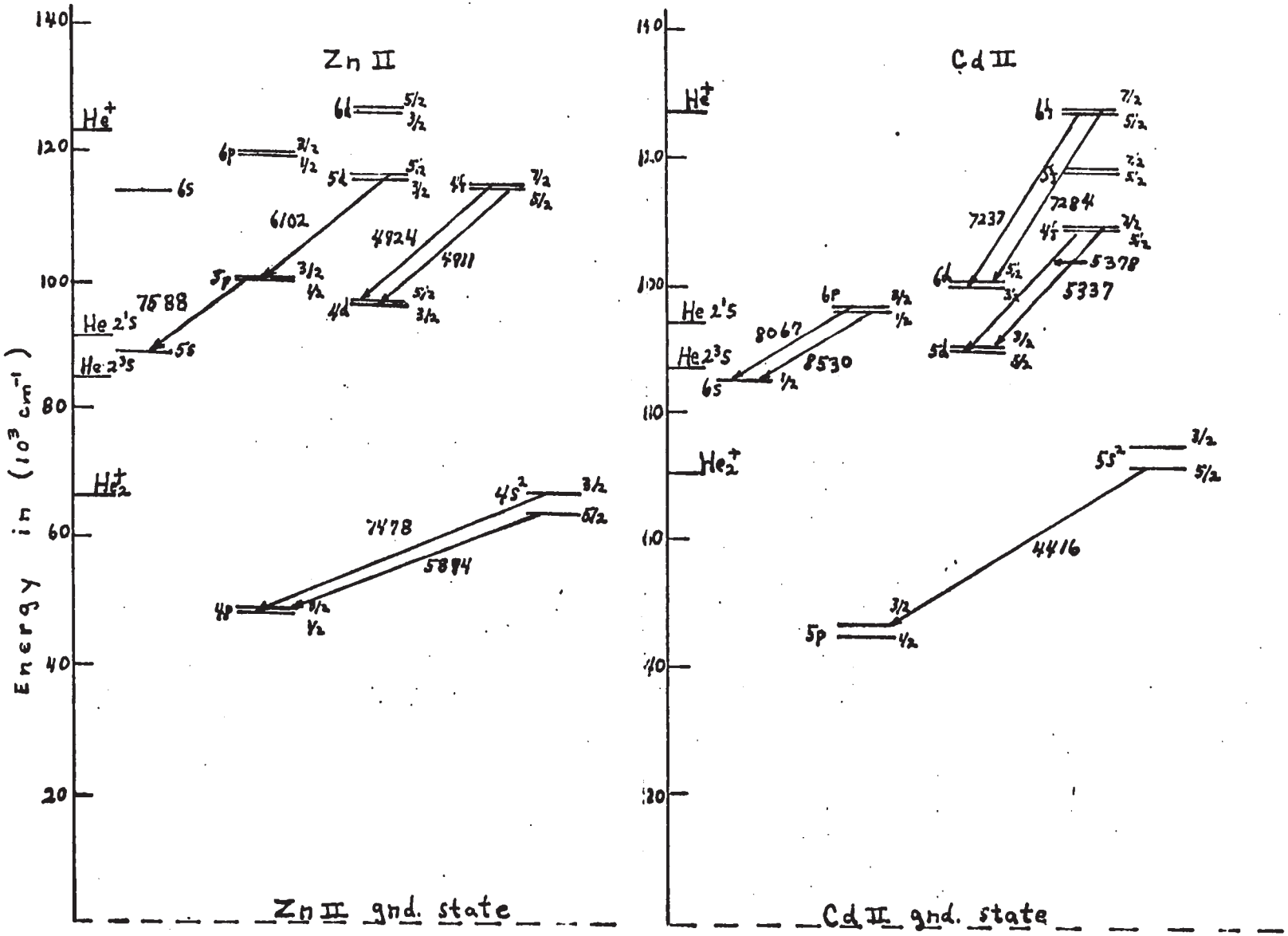
Zn II
Cd II
Energy in (10^3 cm^{-1})
140
120
100
80
60
40
20
He^+
He_2^+
He 2¹S
He 2³S
6s
6p
5d
4f
5p
4d
6102
4924
4911
7588
7478
5884
8067
8530
7237
7284
5378
5337
4416
Zn II gnd. state
Cd II gnd. state

Fig (III-3)

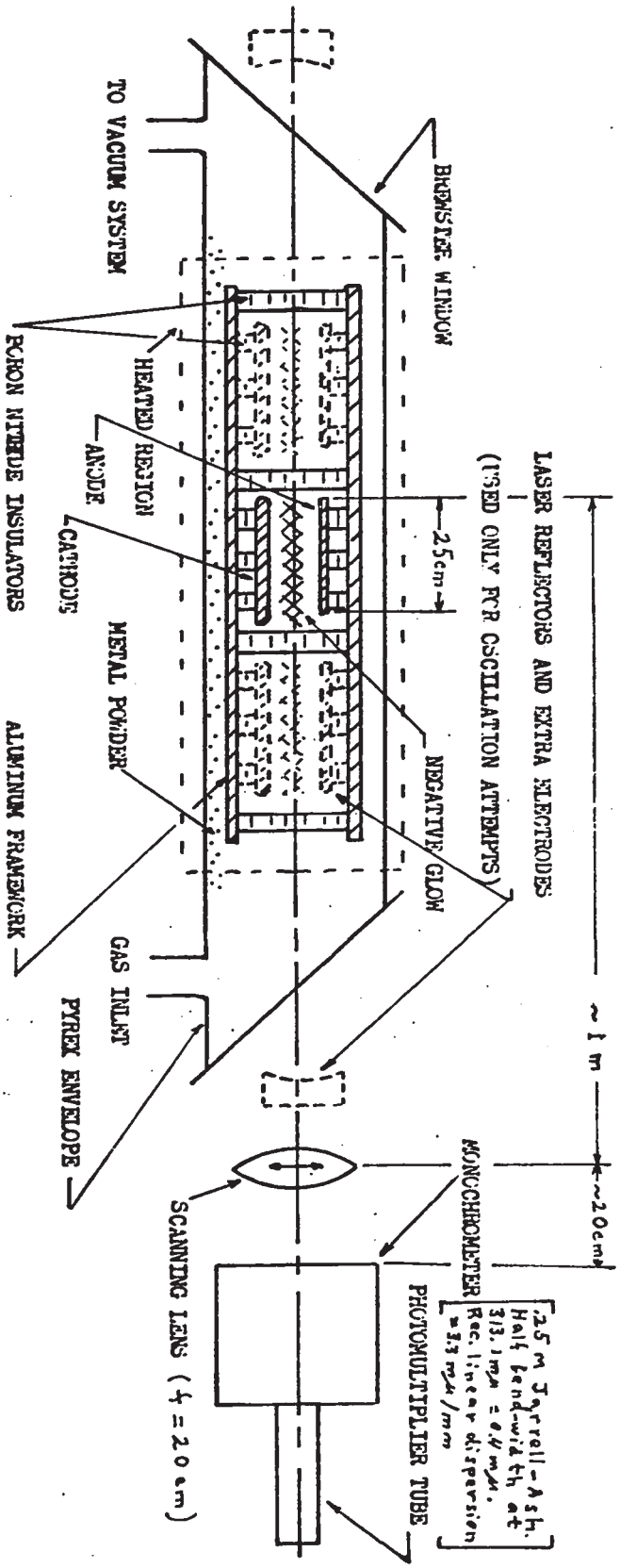
TO VACUUM SYSTEM
BREWSTER WINDOW
LASER REFLECTORS AND EXTRA ELECTRODES
(USED ONLY FOR OSCILLATION ATTEMPTS)
HEATED REGION
ANODE
CATHODE
NEGATIVE GLOW
2.5cm
~1m
~20cm
BORON NITRIDE INSULATORS
METAL POWDER
ALUMINUM FRAMEWORK
GAS INLET
PYREX ENVELOPE
MONOCHROMETER
PHOTOMULTIPLIER TUBE
SCANNING LENS (f = 20cm)

Fig (III-4)

configuration for the following important reasons:

1. Due to enhanced ionization efficiencies, the Crookes dark space in hollow cathodes is, for a given current density, of smaller thickness than in open cathodes.
2. The characteristics of open cathodes are simpler and better understood over a much wider range of cathode fall parameters than is the case with a hollow cathode of a fixed diameter.
3. A hollow cathode does not lend itself as well toward having a controllable and homogeneous concentration of metal vapor in the cathode region as does an open cathode.

The discharge tube itself, into which the electrode framework could be inserted and withdrawn freely, was 2-inch I.D. Pyrex with brewster angle end cutts. Metal powder was placed along the inside of the tube wall and heating of the region indicated in Figure III-4 was accomplished with Heat-by-the-Yard heating tape with a maximum capability of heating the tube to 400°C. Two layers of asbestos tape were used to provide insulation of the heated region sufficient to allow internal temperature to be read to an accuracy of about 5° with thermometers inserted under the

heating tape.

III.3-2: Optics

The arrangement of optical components is also illustrated in Figure III-4. In observing the spontaneous emission characteristics of the discharge, the laser mirrors were, of course, not in place. Also, for these studies, only the central cathode was used. This served to minimize longitudinal temperature gradients and to provide a sharper image of the discharge light on the monocrometer slits.

With such an arrangement, we were able to obtain a clear image of the cathode region at the monocrometer slits showing clearly the cathode surface, Crookes dark space, negative glow, and Faraday dark space. To obtain the profile measurements a transverse movement of the lens provided scanning of these regions across the monocrometer slit. For transferse displacements which are small compared to the lens diameter, which was the case, this is equivalent to moving the slit across the image.

III.3-3: Results

a.) Electrical. By adhering to such standard practices as using highly polished cathode surfaces, baking the

discharge tube under vacuum at close to 400°C, and increasing the discharge voltage gradually prior to discharge experiments, we were able to achieve reproducible abnormal cathode fall behavior in the pure gasses He, Ne, and N_2. If allowance is made for discharge heating, the electrical behavior is found to conform generally with Von Engle's theory.[13] The discharge voltages were ranged between 150 and 550 V, and pressures were usually within 1-10 Torr.

Although no quantitative comparisons were made, the electrical characteristics under the strongly abnormal cathode fall conditions ($V_c \sim 350V$) were found not to be sensitive to the metal vapor concentration up to a temperature of 400% for Zinc and to about 300% for Cadmium. When the Cd temperature exceeded 300% the discharge became unstable and collapsed to a very intense glow on a localized region very close to the cathode surface and usually near the point where the electrical connection was made to the cathode. This instability is evidently brought about by field and temperature inhomogeneities.

b.) Spectroscopic. The most immediately apparent aspect of the spectral characteristics in the cathode region was that the Crookes dark space remained dark as metal vapor was introduced. The spontaneous emissions from

the charge-transfer excited laser transitions appeared to emanate solely from the negative glow region. The profile measurements of individual line intensities in the He-Zn system were, however, much more revealing. The results of these measurements are shown in Figure III-5. The curves are normalized for equal intensities at the 3mm position which is near the peak intensity position for many of the lines.

In obtaining the profile data our procedure was to set the monocrometer at peak intensity for the line in the negative glow and then make repeated scans with the lens. Intensity readings were taken at seven settings of the lens. A slight drifting of the discharge current of no more than 5% would occur during a given scan and was the dominant source of error for these measurements.

The profiles can be regarded as having only relative significance due to the curvature of the negative glow around the cathode ends and to focusing limitations of the lens. However, it is quite evident from the curves that there exist two types of profiles: a normal type which rises smoothly to a maximum at some position within the negative glow, and an abnormal type which exhibits an anomalous bump in the slope near the negative glow boundary.

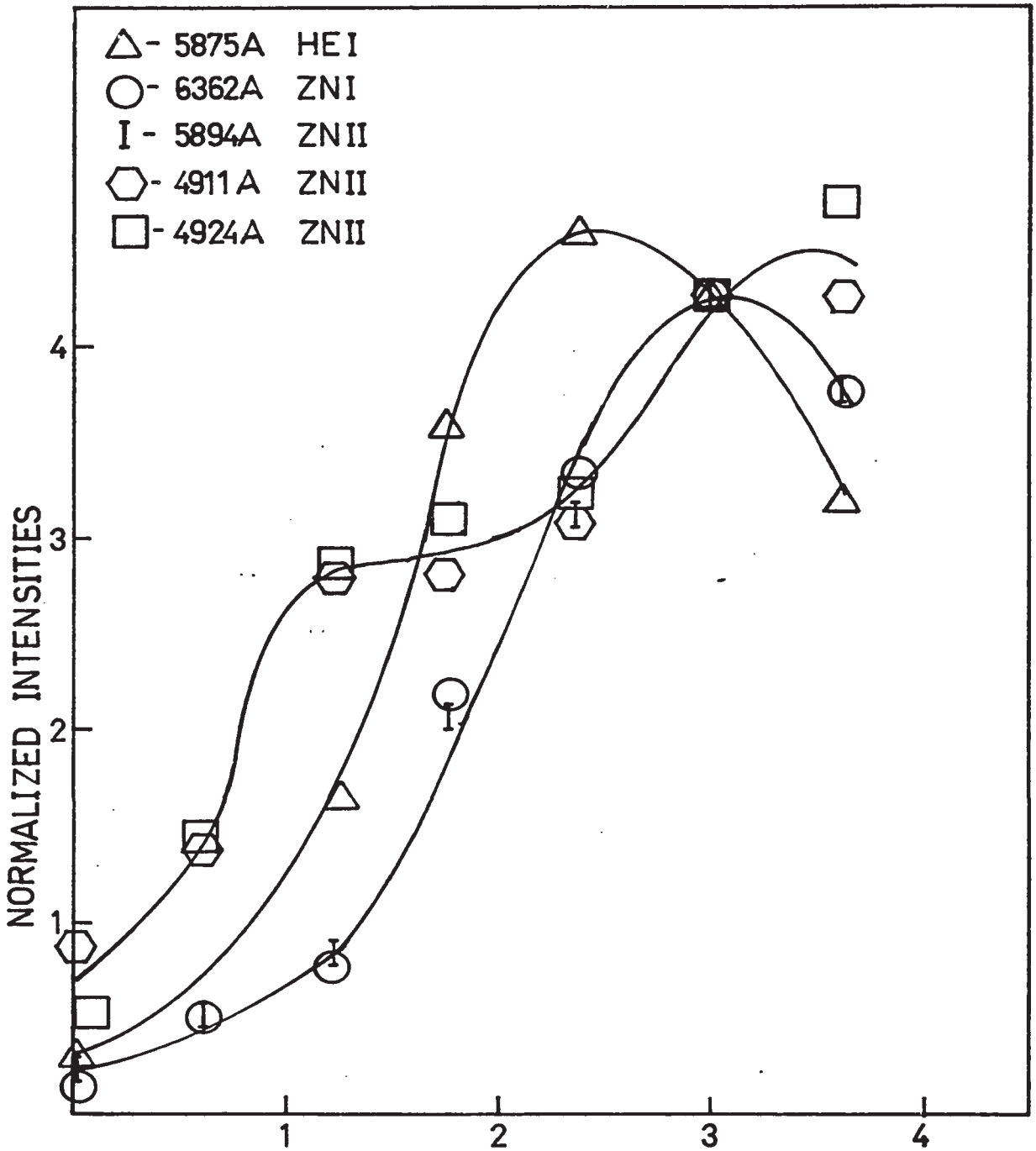
△- 5875A HEI
○- 6362A ZNI
I - 5894A ZNII
⬡- 4911A ZNII
□- 4924A ZNII
NORMALIZED INTENSITIES
1
2
3
4
1
2
3
4
DISTANCE FROM CATHODE (mm)

Fig (III-5)

The two profiles belonging to the latter type are, in fact, of the ZnII laser lines which are suspected to be excited by the charge-transfer reaction (I-1). Other suspected charge transfer excited lines at 7588, 6102, and 6021A were too weak to obtain meaningful profiles. Note that the 5894A line which is now believed to be excited mainly by He metastables exhibits a normal profile. (The 7478A line also exhibited a normal profile.)

The normal profile of the 6362A ZnI line is included as evidence that the anomalous profiles do not result from a Zinc vapor concentration gradient. Similarly, the normal profile of the 5875A HeI line, which requires very nearly as much excitation energy as do the lines which exhibit the abnormal profiles, can be taken as evidence that the abnormal profiles do not result from concentration or temperature gradients associated with the electrons. It is thus legitimate to interpret the anomalous profiles in terms of an effect by the cathode electric field on the Helium ions, and this will be done in Sec. III.4-2.

Profile observations were also made on CdII lines in a He-Cd discharge. All lines scanned, including the 8067A and 8530 laser lines which may be expected to result from charge-transfer,[11] were found to have normal profiles.

We comment on this result in Section III.4-2.

The temperature dependence of the relevant line intensities in the He-Zn and He-Cd systems is shown in Figure III-6. The intensities were measured at the position of peak intensity within the negative glow. The discharge current was kept at a constant value, and to insure negligible heating by the discharge this value was chosen low enough such that the similarity relation j/p^2 = const. held true. The behavior is seen to be similar to the positive column and points to the need for re-examining our assumption regarding ionization by predominantly high average energy electrons.

c.) Oscillation. Several unsuccessful attempts were made to obtain c.w. oscillation of the 7478A and 7588A line in He-Zn and the 5378A and 4416A lines in He-Cd. For this purpose, all three cathodes were used giving the discharge region an effective length of 75cm. Tube temperature was set at the value for maximum spontaneous emission of the laser lines, and He pressure and discharge current were ranged roughly over 1-10 Torr and 0-.6 amp, respectively. The mirrors provided 99.8% reflectivity at 7478A, 7588A, 5378A, and 97% at 4416A.

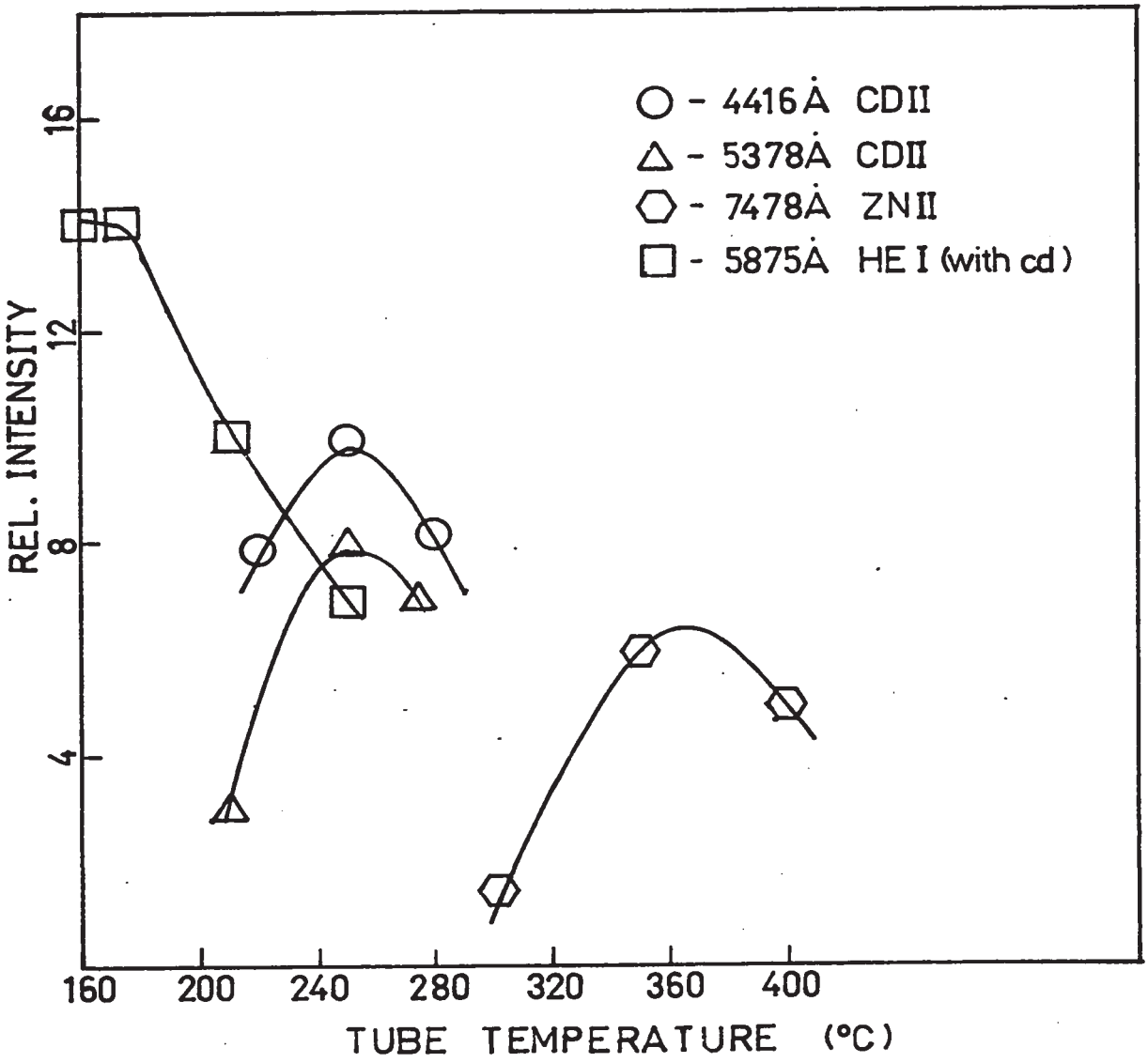
○ - 4416 Å CDII
△ - 5378 Å CDII
⬡ - 7478 Å ZNII
□ - 5875 Å HE I (with cd)
REL. INTENSITY
4
8
12
16
160
200
240
280
320
360
400
TUBE TEMPERATURE (°C)

Fig (III-6)

III.4: INTERPRETATION OF RESULTS

The above results, while having limited quantitative value, are of considerable importance in helping us to formulate a model of the cathode region in metal vapor - rare gas glow discharges than is presently available and allows us to assess more confidently the suitability of the cathode region as an environment for charge-transfer excited laser action. Below, we adopt a simplified one-dimensional model of the negative glow and dark space which allows a satisfactory interpretation of the qualitative features of our observations.

III.4-1: Quenching of Rare Gas Ion Production in the Negative Glow

We make the following assumptions with regard to the negative glow:

1. Consistent with the probe measurements of Pringle and Farvis[16] the electrons are assumed to fall into three groups: the primary, secondary, and ultimate electron groups. The primary electrons are those which have entered the negative glow from the Crookes dark space with an average energy close to the cathode potential fall. The secondary group is ejected electrons resulting from ionization by

the primary group and have a fixed average energy of around 5 ev.[16] The ultimate group is characterized by a Maxwellian energy distribution at a temperature which depends sensitively on the discharge conditions. The ultimate electrons, which are by far the most numerous of the three groups, are assumed to be primary and secondary electrons which have reached an equilibrium state after undergoing successive collisions.[16]

2. For simplicity we assume a homogeneous distribution of all three groups throughout the negative glow.
3. Ion and electron losses are due to diffusion. Even with the use of the rather large dissociative recombination coefficient relevant to Helium ($\rho \sim 10^{-9}$ cm^3/sec at $T_e \sim 1$ ev)[13] this assumption is valid for the open cathode situation with negative glow dimensions on the order of 1cm or less. Its range of applicability thus includes both our discharge and that used in Ref. 16. There is evidence that recombination becomes an important loss mechanism for negative glows of much larger dimensions and it may also be important in the hollow cathode configuration where the electrons

become trapped by the cathode field.

It is obvious that in order to explain the quenching of the production of rare gas ions, one needs a balance equation analogous to eq.(II-11) for the positive column. The balance equations relevant to the above model or the negative glow are as follows (in a pure gas):

Balance equation for ions:

$$(Z_p n_p + Z_s n_s + Z_u(T_e) n_u) p = -\frac{D_+}{p} \frac{d^2}{dx^2}(n_+) \qquad \text{(III-13)}$$

Balance equation for secondary electrons:

$$(Z_p n_p) p = \gamma n_s n_u - \frac{D_-}{p} \frac{d^2}{dx^2}(n_s) \qquad \text{(III-14)}$$

Balance equation for ultimate electrons:

$$(Z_s n_s + Z_u(T_e) n_u) p + \gamma n_s n_u = -\frac{D_-}{p} \frac{d^2}{dx^2}(n_u) \qquad \text{(III-15)}$$

where,

Z_p is the ionization coefficient at unit pressure for the primary electrons.

Z_s is the ionization coefficient at unit pressure for the secondary electrons.

Z_u is the ionization coefficient at unit pressure for the ultimate electrons.

D_+ is the diffusion coefficient at unit pressure for

ions.

D_- is the diffusion coefficient at unit pressure for electrons.

γ is a rate coefficient for thermalization of secondary electrons with ultimate electrons.

n_p is the concentration of primary electrons.

n_s is the concentration of secondary electrons.

n_u is the concentration of ultimate electrons.

n_+ is the concentration of ions.

P is the pressure.

It is consistent with the data of Pringle and Farvis[16] to make the following two approximations:

1. The term representing ionization by primary electrons can be neglected in the balance equation for ions.

2. We may put $n_+ \sim n_s + n_u \sim n_u$

Further, we may make the following approximations:

3. The primary electrons undergo multiplication in the dark space by a factor $\exp(\eta V_c)$. Incorporating into Z_p the initial electron concentration at the cathode, we write:

$$n_p = \exp(\eta V_c)$$

4. We assume that the spatial density gradients in the negative glow remain constant at a constant current density. We put,

$$d^2/dx^2 \approx -\delta^{-2} \qquad \text{(III-16)}$$

where δ is roughly the thickness of the negative glow. (As in the case with the positive column, we anticipate here more sensitive dependencies through exponential factors to justify this approximation for qualitative results.)

5. Over the range of pressures of interest it can be shown that diffusion is the dominant loss mechanism for the secondary electrons, so we neglect the first term on the right hand side of eq.(III-14).

With these approximations our balance equations are left in the form:

$$(Z_s n_s + Z_u n_u) P = \frac{D+\delta^{-2}}{P} n_u \qquad \text{(III-17)}$$

$$Z_p \exp(\eta V_e) = \frac{D-\delta^{-2}}{P^2} n_s \qquad \text{(III-18)}$$

$$(Z_s n_s + Z_u n_u) P = \frac{D-\delta^{-2}}{P} n_u - \gamma n_s n_u \qquad \text{(III-19)}$$

Thus we have three equations and four unknowns: n_s, n_u, V_e, and T_e. A fourth equation is obtained by using the fact

that in the absence of a field the discharge current will be carried by diffusion; i.e., we can write:

$$j = f \frac{D_+ \delta^{-1} e}{p} n_+ \qquad \text{(III-20)}$$

where f is a geometrical constant less than one. Approximation No. 2 allows us then to write:

$$\frac{D_+ \bar{\delta}^{-2} n_u}{p} \simeq C \qquad \text{(III-21)}$$

where C is a constant depending only on j.

At this point we should compare the general behavior predicted by this model with some of the observations made by Pringle and Farvis.[16] They observe, for example, that the density of ultimate electrons is roughly proportional to the current density and to the pressure at constant current density. Our equation (III-21) is consistent with these observations. They also observed that while the ultimate electron group contributes insignificantly to ionization compared to the secondary group, the electron temperature of the ultimate group falls rapidly with increasing pressure similar to the behavior which occurs in the positive column. This rather puzzling behavior is, as we now show, also explained by our model.

We combine equations (III-17), (III-18), (III-19), and

(III-21) to obtain two equations with two unknowns: V, and T_e:

$$[a \exp(-\eta V_e) + b Z_u(T_e)] P^2 = c \qquad \text{(III-22)}$$

$$[a \exp(-\eta V_e) + b Z_u(T_e)] P^2 = B - \gamma' \eta (V_e) P^2 \qquad \text{(III-23)}$$

where $a = \frac{Z_g Z_p}{D_- \delta^{-2}}$, $b = c D_+^{-1} \delta^2$, $B = \frac{D_-}{D_+} c$, and $\gamma' = \frac{\gamma Z_p c}{D_- \delta^{-2} D_+}$.

Eliminating $\exp(-\eta V_e)$ we obtain:

$$Z_u(T_e) = E/P^2 \qquad \text{(III-24)}$$

With $E = \frac{c + a/\gamma' (c - B)}{b}$.

Equation (III-24) is seen to be of the same form as equation (II-4) describing the dependence of the positive column electron temperature on pressure.

What occurs physically is that ionization by the ultimate electrons balances the injection of new ultimate electrons resulting from the thermalization of the secondary group.

We now focus our attention on another important prediction of the model. According to equations (III-24) and (III-22), if ionization by secondary electrons is dominant at one pressure, as it is observed to be for He at ~ 0.5

Torr,[16] then at constant current density it will be dominant at a higher pressure, such as was used in our experiment. In examining the response of the production rate of He ions to the relative concentration of metal vapor, we therefore neglect the second term in the brackets of equation (III-22). Representing by a factor R, again, the relative concentration of metal vapor and by $Z_{s_{He}}$ and $Z_{s_{M.V.}}$ the secondary ionization coefficients for He and the metal vapor, we have an equation of the form:

$$(Z_{s_{He}} + R Z_{s_{M.V.}}) \exp(\eta V_c) = \frac{c(i)}{p^2} \qquad \text{(III-25)}$$

where we have also made use of the fact that the production rate of secondary electrons will remain insensitive to R. This is the desired equation analogous to eq.(II-11) for the positive column. Like eq.(II-11), it predicts that the production of He ions will begin to drop as r approaches a value which makes the two terms in the brackets of comparable value. This is effected by a drop in V_c of only a few percent, which was not monitored in the experiment. The (fixed) energy distribution of the secondary electrons which enters in Z_s has been observed to be roughly Maxwellian[16] with an average energy of $\sim$ 5eV, which is close to the electron temperature in the positive column

lasers. Therefore, after comparing eq.(II-11) with eq. (III-25), one expects quenching to occur at a metal vapor concentration comparable to that of the positive column, and this is consistent with our observations. An exact calculation of the position of the relevant maximums as a function of R requires more detailed information than is available from the model in its current oversimplified state.

It is interesting to note also that this model predicts a $1/R$ dependence of the production of rare gas ions at constant j while in the positive column a $(1/R)^{V_1/V_2}$ dependence is predicted where V_1 and V_2 are the ionization potentials of the rare gas and metal vapor, respectively. A more controlled experiment may be capable of detecting this difference. Also, this may account in part for the maximums occurring at a slightly higher temperature than in the positive column.

In the case of hollow cathodes or large negative glow volume-to-surface ratios where recombination becomes important it may happen that ionization by the ultimate electron group becomes dominant over that by the secondary group. We do not consider this case explicitly here but merely point out that quenching will then occur simply as a result

of a cooling effect on the ultimate electrons similar to what occurs in the positive column.

III.4-2: Profiles

The geometry of the above model in combination with an assumed linear form for the field in the dark space also permits a qualitative interpretation of the anomalous profiles of Figure III-6.

In Figure III-7 we have divided the cathode region into parts. Regions I - III define the Crookes dark space and contain an electric field which increases linearly from zero at the negative glow boundary to a maximum at the cathode surface. The production rate, Z, of the excitation carrier ions in these regions is assumed equal to zero. Z is assumed constant in the negative glow (region IV). With the excitation rate of the charge-transfer excited lines known to take the form:

$$R \propto N_+ \cdot \bar{V} \qquad \text{(III-26)}$$

where $\bar{V}$ is the larger of $V_{thermal}$ or V_{drift}, we may discuss the profiles on the basis of the steady state equation of continuity for the ions:

$$\frac{d}{dx}\left[N_+ (\bar{V}_{diff.} + \bar{V}_{drift}) \right] - Z = 0 \qquad \text{(III-27)}$$

I	$k_+ E/P > Vth$	$Z = 0$
II	$Vth > k_+ E/P > Vdiff.$	"
III	$k_+ E/P \sim Vdiff$	"
IV	$E/P = 0$	$Z = const.$

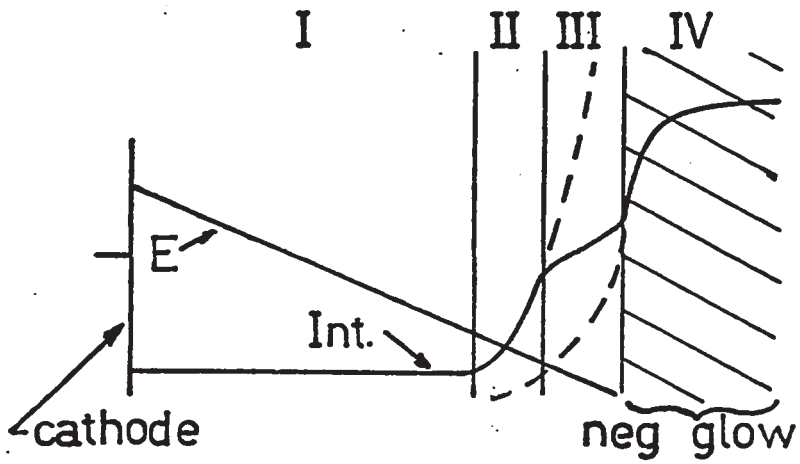

Fig (III-7)

where V_{diff} is the average diffusion velocity of the ions. The classification, below, of the three regions within the dark space according to the value of the ion drift velocity, facilitates the analysis:

Region I: Here, $\bar{V}_{drift} > \bar{V}_{thermal}$ $(> V_{diff})$ and the continuity equation requires d/dx (R) = 0. (III-28)

Region II: Here, $\bar{V}_{thermal} > \bar{V}_{drift}$, and we have $R \propto N_+ \bar{V}_{th}$. With the assumed linear form for E, the continuity equation becomes:

$$d/dx[\, N_+ k_+ E_o (x-x_o)\,] = 0 \qquad \text{(III-29)}$$

(k_+ is the ion mobility)

or

$$N_+ = \text{const.}/(x-x_o) \qquad \text{(III-30)}$$

and since $\bar{V}_{th.}$ is constant, we have,

$$R = \text{const.}/(x-x_o). \qquad \text{(III-31)}$$

Region III: With $\bar{V}_{drift} < \bar{V}_{thermal}$, we again have $R \propto N_+$. Here we assume $\bar{V}_{drift} \sim \bar{V}_{diffusion}$. Rather than solve the continuity equation with both diffusion and field contributions to the ion velocity present, we consider

alternatively the two cases $\bar{V}_{diff} < \bar{V}_{drift}$ and $\bar{V}_{diff} > \bar{V}_{drift}$. The first case is of course the same as in region II, and the solution is represented by the dotted extension of the profile of region II into region III. The continuity equation for the second case becomes:

$$- D_+ \, d^2/dx^2 \, (N_+) + N_+/\tau = 0 \qquad \text{(III-32)}$$

where D_+ is the ion diffusion coefficient and τ is the lifetime of the ion due to asymmetric charge-transfer. The solution is

$$N_+(x) = N_+(x_o) \exp[-\alpha(x-x_o)] \qquad \text{(III-33)}$$

with $\alpha = (D_+\tau)^{-1/2}$, and is represented by the other dotted profile in region III. The actual profile for $\bar{V}_{diff} \sim \bar{V}_{drift}$ is shown as being intermediate between these two limiting cases.

Region IV: Here again, $R \propto N_+$. The continuity equation in this region is written as:

$$- D_+ \, d^2/dx^2 \, (N_+) + N_+/\tau - Z = 0 \qquad \text{(III-34)}$$

The appropriate solution is:

$$N_+(x) = N_+(0) + N_+(x_o)[1 - \cosh \alpha x] \qquad \text{(III-35)}$$

$N_+(0)$ is arbitrary and $N_+(x_o)$ is determined by requiring continuity of the solution across the III - IV boundary.

The composite profile, derived by smoothly connecting these individual profiles, is shown in Figure III-7. It is seen to resemble qualitatively the anomalous profiles of Figure III-6.

At this point we will offer two possible explanations for the absence of anomalous profiles in He-Cd. Firstly, they may be related to a stronger degree of Penning ionization occurring in this system relative to the He-Zn system. A recent report[17] shows the cross sections for the Penning reactions greater in a factor of 3 in the He-Cd system than in the He-Zn system. Such ionization by metastables may effectively widen the negative glow into Region III due to metastable drift into this region and thus obscure the effect of the field on the ion excited lines in this region.

Secondly, it may be due to a dominance of electron collisional excitations of the lines which were looked at.

While the levels which are assumed to be directly excited by charge-transfer are even more closely resonant to the Helium ionization potential than are the corresponding levels of Zinc, the only relevant transitions which were strong enough in our discharge to make profile observation on (8067A and 8530A) were from levels which required at least two cascade transitions from the near-resonant levels. (See Fig. III-3, supra.)

The model profile in Figure III-7 has, of course, not been drawn to scale. It is important to have an order of magnitude idea of how the intensity of the charge-transfer excited lines in the dark space compares to that in the negative glow. The maximum intensity ratio will occur for $\alpha D_+ >> 1$. In this case, the continuity equation gives:

$$I_{n+}(I)/I_{n+}(IV) \sim \bar{V}_{diff}/\bar{V}_{th} \sim 10^{-2} \qquad \text{(III-36)}$$

This low value is not incompatible with our observations. As previously mentioned, it was not possible, with our optics, to resolve such intensity differences.

On the other hand, the transverse scale of the profiles does present some difficulties. Using the assumption that the field grows linearly from zero to a typical 1000 V/cm at the cathode, one estimates that the width of Regions II

and III should be on the order of 1/10 the width of Region I. Obviously this does not conform with our observations which indicate that the anomalous portion of the profiles extend over a width of the same order as that of the dark space. However, the basic explanation of the shape of the anomalous profiles will remain valid if one simply replaces the hypothetical infinitely sharp boundary between Regions III and IV by a more reasonable buffer zone wherein the field is intermediate between zero and the fast-rising value it attains in the dark space. Such a buffer zone, which obviously does exist in real life, would also be characterized by a spatially dependent Z. It is not unreasonable to expect this zone to have a width comparable to that of the dark space.

III.4-3: Oscillation

We are now in a better position to evaluate the cathode region as a practical environment for charge-transfer laser excitations. In particular, we can interpret the negative results in our attempts at achieving oscillation in the cathode region.

We have seen that, due to a quenching action similar to what occurs in the positive column, the metal vapor concen-

tration is limited to $\sim 10^{-14}$ for practical operating conditions in the cathode region. Under these conditions, according to eq.(III-8), a discharge current density of $\sim 10^{-2}$ amps/cm^2 is required to achieve threshold for laser action in He-Zn in the Crookes dark space. Our power supply limited us to discharge currents far below this value in our attempts at oscillation.

On the other hand, according to eq.(III-36), the threshold current density for laser action in the negative glow was exceeded in these attempts. We now point out several factors which could account for our not observing laser action in the negative glow.

One of the most important factors is believed to be the effect of discharge heating. The onset of discharge heating effects, determined by departures from the similarity relation, $j/P^2 = \text{const}$, were noticed at current densities of the same order of magnitude as the threshold value required by equations (III-8) and (III-36) for laser action in the negative glow. Rough calculations have been carried out which indicate that concentration gradients across the discharge region resulting from discharge heating could amount to $\sim$ 100% at the discharge currents used in our attempts at achieving oscillation. An important advantage

of the hollow cathode lasers which derive the metal vapor through either sputtering or discharge heating is that such concentration gradients arising with increasing current density will tend to be opposed by the increased metal vapor pressure.

Other possible factors contributing to our negative results include:

1. Competing lower level excitations or bottleneck processes occurring in the negative glow which would not permit c.w. inversions to be maintained.
2. Optical inhomogeneities due to temperature gradients and/or cathode alignment distortions arising at the high temperatures.
3. Condensations on the brewster windows. While the metal vapor condensations could be removed by the use of internal heating coils, a compound was found to form slowly on the windows which could not be so removed.

CHAPTER IV

OBSERVATIONS ON THE CATHODE REGION OF A TRIODE DISCHARGE

Within the context of the model presented in section III.4-2, it can be shown that if the quantity $(\chi_0 \alpha)^{-1}$ is less than one, then the intensity of charge-transfer excited emission in the Crookes dark space should be roughly proportional to this quantity. Now $\alpha^{-1} = (D_+ \tau)^{1/2}$ and is a measure of the average displacement which an excitation carrier ion (e.g. He^+) will undergo in the negative glow due to diffusion before being converted through charge-transfer to a metal vapor ion, the latter process occurring at the rate τ^{-1}. Under conditions appropriate to our discharge observations ($P \sim 6$ Torr , $T_{gas} \sim 360°C$) the quantity α^{-1} is estimated to be ~ 0.1 cm. ($D_+ \sim 10^2$ cm^2/sec is obtained from ref.(13,p.119), and $\tau \sim (\sigma_{ct} \cdot n_{Zn} \cdot \bar{v}_{th})^{-1} \sim 10^{-4}$ sec is calculated from the charge-transfer cross sections, $\sigma_{ct} \sim 2 \cdot 10^{-15}$ cm^2 reported in ref.(6).) With the observed width of the negative glow taken as $\chi_0 \sim 0.3$ cm, we see that $(\chi_0 \alpha)^{-1} < 1$ and the possibility appears of enhancing the emission in the Crookes dark

space through a reduction of α, i.e. by reducing the average time it takes an ion to traverse the width of the negative glow. While the above considerations obviously do not apply in the case where a significant amount of ion production occurs in a buffer zone containing a finite field, it should at least be possible to gain more information about such a buffer zone by examining the response of the anomalous profiles to induced changes in α .

One method of reducing α might be to impart a field-induced drift velocity to the ions in the negative glow. Using the known value of the mobility of He^+ ions, a field strength in the negative glow of only $\sim$ 2 V/cm would be required to bring $(\gamma_0 \alpha)^{-1}$ near unity. This approach is what motivated the construction of the triode discharge configuration to be discussed in this chapter. It is now recognized that it is not possible to provide the required field in the negative glow by the use of a grid.

The reason for this will be familiar to anyone with experience in probe diagnostics of plasmas. In plasmas with charge densities exceeding $\sim 10^8$ cm^{-3} any grid or probe placed in the plasma and biased positively or negatively with respect to the plasma potential will develop, respectively, an electron or ion space charge sheath

adjacent to its surface which insulates the rest of the plasma from the grid potential. The sheath thickness is calculated by simply combining Poisson's equation with the assumption that the electrons or ions undergo free fall in the sheath and carry a current density, $j_{\pm} = N_{\pm} \bar{C}_{\pm}$ where $\bar{C}_{\pm}$ is the average electron or ion thermal velocity.[15] For our plasma the result for the relation between the sheath potential fall and thickness is:

$$V^{3/2}/d^2 = \left(\frac{9\pi}{4}\right)\left(\frac{2}{e m_+}\right)^{-1/2} N_+ \cdot \bar{C}_+ \sim 2 \cdot 10^4 \; V^{3/2} cm^{-2}$$

$$V^{3/2}/d^2 = \left(\frac{9\pi}{4}\right)\left(\frac{2}{e m_-}\right)^{-1/2} N_- \cdot \bar{C}_- \sim 6 \cdot 10^5 \; V^{3/2} cm^{-2}$$

for a negatively and positively biased grid, respectively. It is seen that the required uniform field of $\sim$ 2 V/cm throughout a region of width comparable to that of the negative glow cannot be provided by a grid of either bias polarity. Increasing the grid bias to a degree sufficient to cause the sheath width to approach that of the negative glow will simply exclude the negative glow from the sheath region forming a dark layer which will ultimately acquire the properties of the Crookes dark space or anode dark space, as the case may be.

While the above conclusions seem to preclude the grid's acting selectively to enhance the charge-transfer excited

emissions in the Crookes dark space, a very important and rather unexpected effect of the grid on the emissions in the negative glow was observed and will be discussed below.

IV-1: Electrode Configuration

A coaxial electrode configuration was chosen for the triode discharge. Its design is illustrated in Figure IV-1. This design has two important advantages. The cathode geometry eliminates cathode end distortions of the negative glow, and the extension of the length of the grid beyond that of the cathode prohibits the discharge from shunting around the grid. Like the rectangular electrode framework, this electrode assembly could be inserted and withdrawn freely within the 2-inch diameter Pyrex envelope.

IV-2: Observations and Discussion

Due to the presence of the grid shadow on the light coming from the cathode region, it was not possible to make profile measurements which could be compared with those reported in section III.4-2.

Consistent with our conclusions regarding sheath insulation, no selective enhancement of emission from the charge-transfer excited lines in the Crookes dark space was effected by negatively biasing the grid which was posi-

Fig (IV-1)

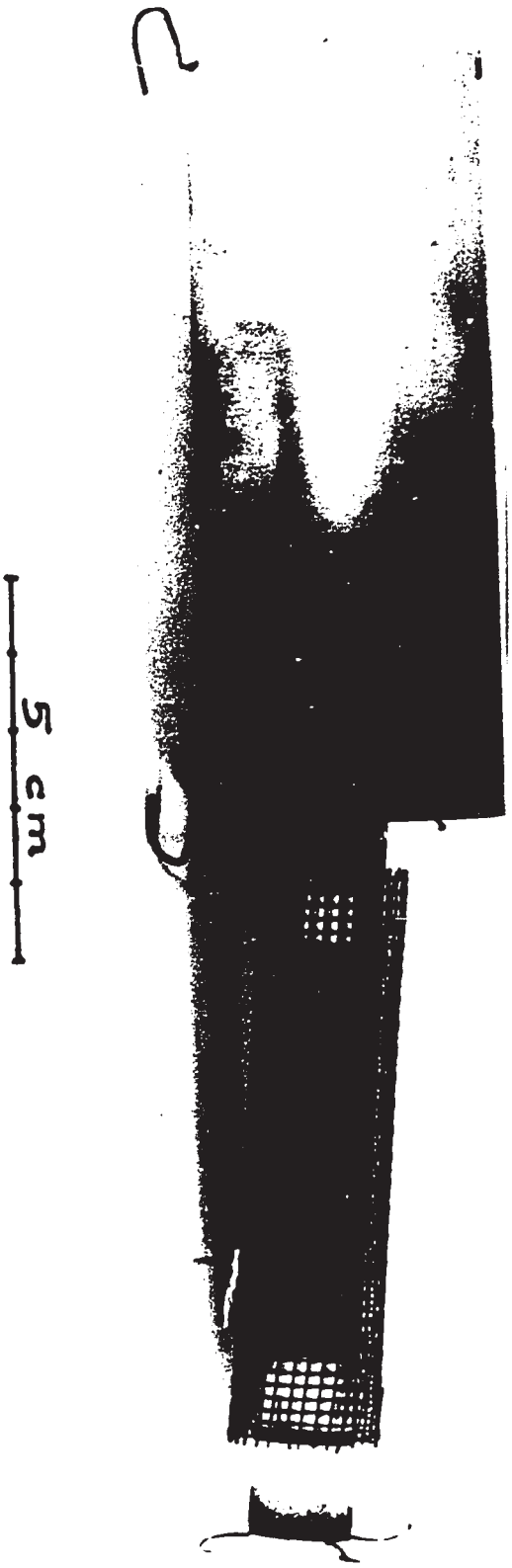

Fig (IV-1)

tioned near the cathode-side boundary of the negative glow. However, a very dramatic enhancement of the emission from all lines occurred in the negative glow. This enhancement occurred for constant cathode current.

Table IV-1 presents the results of the grid enhancement observations in He-Cd. At the 6.5 Torr pressures the negative glow positioned itself such that the grid appeared near its cathode-side boundary. In this situation the cathode voltage had to be reduced by an amount approximately equal to the induced grid voltage change in order to keep the cathode current constant at two milliamps. For the 8 Torr observations the grid appeared to be situated well within the negative glow. Although large enhancements still occurred, the grid bias acted to decrease the cathode current in this case, and the cathode voltage had to be increased slightly in order to maintain constant cathode current. This observation seems to support the view that the enhancement effect of the grid results from secondary electron emission from the grid itself and not from its effect on cathode electrons.

It is also clear from the data that stronger enhancements occur for lines originating from higher energy levels. This, evidently, results from a shift in the

TABLE IV-1

GRID ENHANCEMENT RESULTS FOR THE TRIODE DISCHARGE THROUGH He-Cd

i(cathode) = 2ma

P	V_c	V(grid)	i (grid)	Rel. Intensity			
				CdI 6438A	CdII 4416A	HeI 5875A	CdII 7284A
6.5 Torr	300 volts	18 volts	0 milli-amp.	0.7	1.8	1.4	0.9
6.5	275	45	0.5	1.0	2.6	2.5	1.7
6.5	225	92	1.1	-	4.4	4.8	3.3
8.0	250	16	0	-	-	0.8	-
8.0	260	33	1.8	-	-	1.6	-

electron energy distribution in the negative glow due to the fact that the new secondary electrons are accelerated in the sheath and are introduced into the plasma with an energy which is large relative to the average electron energy in the negative glow.

It is important to realize that these effects are associated with a large increase in efficiency for light generation in the negative glow. We can calculate, for example, the ratio of efficiencies for generating emission at the 7286A laser line for the grid current, i_g, going from zero to 1.1ma at a constant cathode current, i_c, of 2ma (see Table IV-1). The ratio of the efficiencies is,

$$\varepsilon'/\varepsilon = [I'(7286)/ (V_c' i_c' + V_g' i_g)]/[I(7286)/V_c i_c]$$

$$\approx 4$$

where the primed and unprimed quantities refer to when the grid is biased and floating respectively. I(7286) is the relative intensity of radiation in the negative glow at 7286A, and V_c and V_g are the cathode and grid voltages relative to the anode. It seems certain that this increase in efficiency is due, in large measure, to the higher efficiency for producing secondary electrons from a surface immersed in the negative glow relative to the corresponding efficiency at the cathode surface, this being due to the higher rate of collisions with the surface of radiation quanta, ions, and metastable atoms occuring in the negative glow relative to the Crookes dark space.

The above effect is obviously of considerable practical importance in optimizing the efficiency of the recently developed hollow cathode lasers. The incorporation of a grid into these devices would, in addition to providing the enhancements, also provide a means of varying the current density through the negative glow while maintaining a fixed current density to the cathode with the important consequence of being able to keep constant the Crookes dark space thickness. The characteristics of hollow cathode discharges depend sensitively on this latter parameter.

CHAPTER V

COMPUTER CALCULATIONS OF POPULATION INVERSIONS IN THE Ne-Mg SYSTEM

In the previous three chapters we have been concerned mainly with general electrical and collisional aspects of electric discharges through metal vapor - rare gas mixtures under conditions appropriate to charge-transfer excitation of stimulated emission. These considerations have led to an understanding of the dependence of the output power from a given laser transition on discharge conditions. No attempt, however, has yet been made to predict which transitions in a particular system will be inverted.

While the exact dependence of the charge-transfer cross section on energy defect and term value is still unclear, it is generally known that the cross sections are highly resonant to the excitation of levels which satisfy the so-called Massey adiabatic criterion:(18)

$$b\,|\Delta E|/h\nu \approx 1 \qquad \text{(V-1)}$$

where ΔE is the energy defect of the process, v is the

relative velocity of collision, b is the range of interaction of the atoms, and h is Planck's constant. In situations (which may be met in the Crookes dark space and perhaps in other ion beam arrangements) where one can neglect competing excitation processes such as by electron and metastable collisions, and radiation transfer processes, the level populations will result simply from cascade transitions originating from a relatively few levels which satisfy the Massey criterion and are excited by charge-transfer.

In order to calculate the relative level populations which will develop from this process, one needs to know the oscillator strengths of all transitions possible among the levels which lie between the ion ground state and those levels directly excited by charge-transfer. In general, it is not possible to have such a complete knowledge with good accuracy from either experiment or theory. There is, however, at least one system for which oscillator strength calculations of sufficient accuracy are feasible. This is the Neon - Magnesium system.

Energy levels of the Magnesium ion are shown in Figure V-1. As can be seen in that figure, this ion has, first of all, a small group of levels whose energies are very close

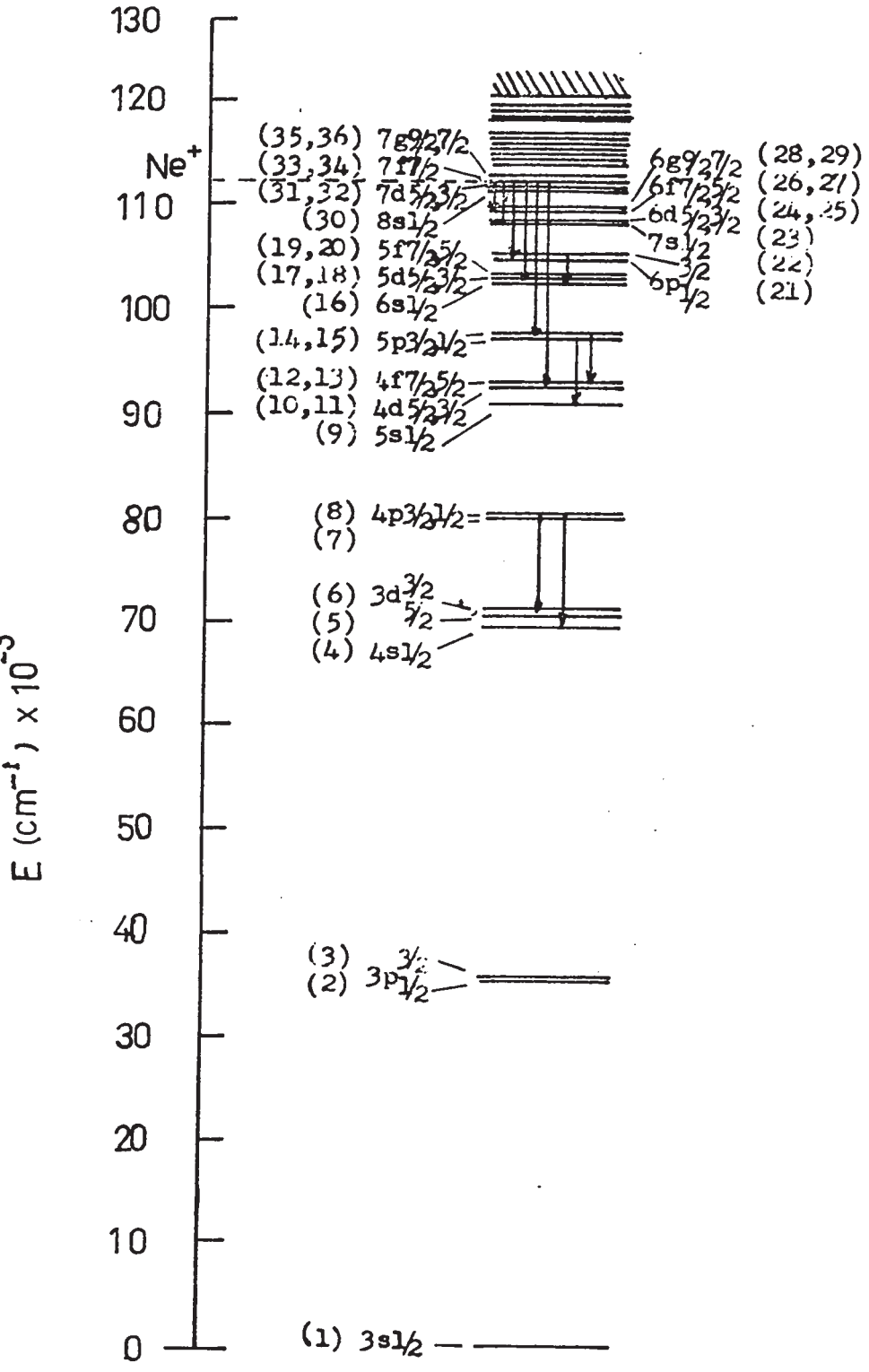
130
120
110
100
90
80
70
60
50
40
30
20
10
0
Ne+
E (cm⁻¹) x 10⁻³
(35,36) 7g9/2,7/2
(33,34) 7f7/2
(31,32) 7d5/2,3/2
(30) 8s1/2
(19,20) 5f7/2,5/2
(17,18) 5d5/2,3/2
(16) 6s1/2
(14,15) 5p3/2,1/2
(12,13) 4f7/2,5/2
(10,11) 4d5/2,3/2
(9) 5s1/2
(8) 4p3/2,1/2
(7)
(6) 3d3/2
(5) 5/2
(4) 4s1/2
(3) 3/2
(2) 3p1/2
(1) 3s1/2
6g9/2,7/2 (28,29)
6f7/2,5/2 (26,27)
6d5/2,3/2 (24,25)
7s1/2 (23)
3/2 (22)
6p1/2 (21)

Fig (V-1)

to the ionization energy of Neon and easily satisfy the adiabatic criterion for an expected large cross section for excitation by charge-transfer. (Δ E should be evaluated at some finite inter-atomic distance corresponding to where the transition occurs. In the absence of information on the shape of the potential curves which this would require, we use, for the sake of argument, Δ E evaluated at infinite separation.) Secondly, the Magnesium ion is alkali-like, having one optically active electron outside a closed shell of core electrons.

Now Bates and Damgaard[19] have developed a technique for calculating oscillator strengths which is based on approximating the actual wavefunctions of the atom or ion by hydrogenic wavefunctions with an effective principal quantum number given by:

$$n_l^* = Z\left[\frac{R}{T_\infty - T_{nl}}\right]^{1/2} \qquad \text{(V-2)}$$

where T_{nl} and T_∞ are the term value and ionization limit, respectively, R is the Rydberg constant, and z is one for neutral atoms, two for singly ionized atoms, etc. The approximation relies on the fact that a major contribution to the transition matrix element comes from regions of r outside of the core where the potential varies as 1/r, and

thus the matrix element should be relatively insensitive to the incorrect behavior of such a pseudo-wavefunction near the origin. In terms of both ease of application and expected accuracy such an approximation is obviously best suited for such one-electron systems as the alkali atoms and group II ions. Also, the approximation obviously becomes more accurate with increasing principal quantum number and, as can be seen from Figure V-1, it is transitions from a set of high lying levels which are most important (i.e., have the lowest branching ratios) for charge-transfer excitation in the Ne-Mg system.

The Ne-Mg system was one of the first systems to be investigated with respect to the enhancement of spark lines by charge-transfer collisions.[20] Its possible application as an ion laser, however, has yet to receive either experimental or theoretical attention. While this system may not be as easy to work with experimentally as some of the other metal vapor - rare gas systems already investigated,[1] the simplicity of the MgII spectrum qualifies it as an excellent system for which to perform population calculations complementary to our theoretical models of the discharge behavior. We devote this chapter, then, to carrying out computer calculations, using the Bates - Damgaard approxi-

mation for the oscillator strengths, of level populations and negative absorption coefficients expected to arise in the Ne-Mg system from charge-transfer and cascade processes.

V-1: Relevant Equations

The steady-state rate equations describing the excitation and cascade processes take the following familiar form:

$$\frac{dN_i}{dt} = R_i + \sum_{j>i} R_{ij} N_j - \frac{N_i}{\tau_i} = 0 \qquad \text{(V-3)}$$

where,

N_i is the population density of the i^{th} level.

R_i is the external excitation rate of the i^{th} level (charge-transfer).

R_{ij} is the radiative transition rate from the j^{th} to i^{th} level.

τ_i is the radiative lifetime of the i^{th} level.

We can write equation (V-3) in matrix notation as follows:

$$\vec{\vec{A}} \cdot \vec{N} = -\vec{R} \qquad \text{(V-4)}$$

where,

$$A_{mn} = R_{mn} \qquad n > m \qquad \text{(V-5)}$$

$$A_{mn} \simeq 0 \qquad n < m \qquad \text{(V-6)}$$

$$A_{mm} = -\tau_m^{-1} = -\sum_{i<m}' R_{im} \qquad \text{(V-7)}$$

The solution for the population densities is therefore:

$$\vec{N} = \overleftrightarrow{A}^{-1} \cdot \vec{R} \qquad \text{(V-8)}$$

The transition rates are expressed in terms of the emission oscillator strengths, F_{mn}, as:

$$R_{mn} = 2 r_0 \, \omega^2/c^2 \cdot F_{mn} \qquad \text{(V-9)}$$

where r_o is the classical electron radius. The negative absorption coefficient is:

$$GAIN = 2(\pi \ell n 2)^{1/2} r_0 \left[N_n - N_m \frac{g_n}{g_m} \right] F_{mn}/\Delta\nu \qquad \text{(V-10)}$$

where g_n & g_m are the level degeneracies and $\Delta\nu$ is the gaussian line width.

For systems satisfying L-S coupling, the emission oscillator strengths can be shown to take the form[21]:

$$F = (1/(2J'+1)) \cdot (4\pi a_o/3\alpha\lambda) S(\ell) S(m) \cdot \sigma^2 \qquad \text{(V-11)}$$

a_o, α, and λ are the Bohr radius, fine structure constant, and wavelength of the line, respectively. $S(\ell)$ and $S(m)$ are the relative line strength and relative multiplet strength, respectively, and are given by,

$$\sigma(\ell) = \frac{(2J+1)(2J'+1)}{2S+1} W^2(LJL'J';S\ell) \qquad \text{(V-12)}$$

$$\sigma(m) = (2S+1)(2L+1)(2L'+1)\ell_>(4\ell_>^2-1)W^2(\ell L\ell'L';L,1) \qquad \text{(V-13)}$$

The primed and unprimed quantities are quantum numbers of the upper and lower state, respectively, $\ell_>$ is the larger of ℓ and ℓ', L_1 is the orbital quantum number of the core, and the Ws are Racah coefficients. σ is the radial matrix element for which the Bates - Damgaard approximation is applied. In this case σ is written in the form:

$$\sigma = \frac{1}{(n^*_{\ell-1}-n^*_\ell)^{3/2}} \left[\int R(n^*_{\ell-1},\ell-1,Z)\, R(n^*_\ell,\ell,Z)\, r\, dr\right]. \qquad \text{(V-14)}$$

The $R(n,\ell,Z)$s are the radial parts of the hydrogenic wavefunctions of effective principal quantum number n^*_ℓ given by equation (V-2). The integral in eq. (V-14) has been tabulated as a function of the variables, $(n^*_{\ell-1}-n^*_\ell)$, n^*_ℓ, Z and ℓ.[21]

V-2: Computer Program

A computer program has been written which calculates, in the above manner, the oscillator strengths for allowed transitions between all the relevant levels of the Mg ion, forms the matrix A, forms A^{-1}, calculates the relative level populations, searches for population inversions, and

calculates the negative absorption coefficients for transitions between the inverted levels. This program appears on pages 79 and 80.

The program operation can be described by numbered sections as follows:

Section 1. Input data are read in. Included are the Racah coefficients, W, level energies, E, and the orbital and total angular momentum quantum numbers, EL and G. PHI is proportional to the radial matrix elements and is read in from tables as a function of the n_i^*s which are calculated in Section 2.

Section 2. The effective principal quantum numbers are calculated using equation (V-2).

Section 3. Oscillator strengths are calculated for allowed transitions using equations (V-11) - (V-14).

Section 4. Radiative transition rates are calculated using equation (V-9).

Section 5. Radiative lifetimes are calculated using equation (V-7).

Section 6. The matrix A is formed using equations (V-5) - (V-7).

```
F40     V21B    8-OCT-70        15:14   PAGE 1

C       TRANSITION RATES AND LEVEL POPULATIONS-MG2
        DIMENSION F(36,36), E(36), EL(36), EN(36), G(36),
       1WJ(0/4,1/5,0/4,1/5), WL(0/4,0/4,0/4,0/4), A(36,36)
       2,R(36,36), B(36,36), ENN(36), PHI(192),S(36)
        DATA WJ(0,1,1,1),WJ(1,1,0,1),WJ(0,1,1,2),WJ(1,2,0,1)/4*.408/,
       1WJ(2,3,1,2),WJ(1,2,2,3)/2*.224/,WJ(2,2,1,2),WJ(1,2,2,2)/2*.091/,
       2WJ(2,2,1,1),WJ(1,1,2,2)/2*.289/,WJ(3,4,2,3),WJ(2,3,3,4)/2*.154/,
       3WJ(3,3,2,3),WJ(2,3,3,3)/2*.040/,WJ(3,3,2,2),WJ(2,2,3,3)/2*.183/,
       4WJ(4,5,3,4),WJ(3,4,4,5)/2*.118/,WJ(4,4,3,4),WJ(3,4,4,4)/2*.022/,
       5WJ(4,4,3,3),WJ(3,3,4,4)/2*.134/
1       DATA WL(0,0,1,1),WL(1,1,0,0)/2*.577/,WL(1,1,2,2),WL(2,2,1,1)/2*
       1.258/,WL(2,2,3,3),WL(3,3,2,2)/2*.169/,WL(3,3,4,4),WL(4,4,3,3)/2*
       2.126/
        READ(5,2)(E(I),I=1,36)
        READ(5,3) (EL(I),I=1,36)
        READ(5,3) (G(I),I=1,36)
        READ(5,4)(PHI(I),I=1,192)
    2 FORMAT (8F10.1)
    3 FORMAT(36(F1.0,1X))
    4 FORMAT(13F6.3)
        DO 7 I=1,36
        DO 6 J=1,36
        A(I,J)=1.E-4
    6 R(I,J)=1.E-4
    7 CONTINUE
        L=0
2       DO 17 I=1,36
   17 EN(I)=2.09/SQRT(1.212674-E(I))
        DO 28  M=2,36
        K=M-1
        DO 27  N=1,K
        L1=EL(M)
        L2=EL(N)
        J1=(G(M)+1.)/2.
        J2=(G(N)+1.)/2.
        DELL=ABS(EL(M)-EL(N))
        DELG=ABS(G(M)-G(N))
        IF(DELL .NE. 1.)  GO TO 27
        IF (DELG .GT. 2.1) GO TO 27
        IF(EL(M)-EL(N))  30,30,31
3   30 GR=EL(N)
        ENL=EN(N)
        ENS=EN(M)
        GO TO 33
   31 GR=EL(M)
        ENL=EN(M)
        ENS=EN(M)
   33 CONTINUE
        DIF=ENS-ENL
        L=L+1
        F(M,N) = 0.166*(E(M)-E(N))*(G(N)+1.)*(2.*EL(M)+1.)*(2.*EL(N)+1.)
       1*GR*                (WJ(L1,J1,L2,J2))**2*(WL(L1,L1,L2,L2))**2
       2*ENL**2*(ABS(ENL**2-GR**2))
```

```
F40     V21B     8-OCT-70          15:14    PAGE 2

4 E     R(M,N)=0.667E10*(E(M)-E(N))**2*F(M,N)*(PHI(L))**2
6 E     A(M,M)=R(M,N)
        WRITE(6,51)M,N,R(M,N)
   51   FORMAT(14,I3,E15.3)
   27   CONTINUE
   28   CONTINUE
        S(1)=1.E+6
        DO 54 N=2,36
5       S(N)=0.
        K1=N-1
        DO 53 I=1,K1
        S(N)=S(N)+R(N,I)
   53   CONTINUE
   63   FORMAT (14,E15.3)
   54   CONTINUE
        DO 62 N=1,36
6       A(N,N)=-S(N)
   62   WRITE(6,63) N,A(N,N)
        EPS=1.E-7
7       N=36
        CALL INVE(A,B,N,EPS)
        DO 65 M=1,36
        ENN(M)=B(M,36)+B(M,35)+B(M,34)+B(M,33)+B(M,32)+B(M,31)+B(M,30)
8       ENN(M)=-1.E+16*ENN(M)
   65   WRITE (6,69) M,ENN(M)
   69   FORMAT (14,E15.3)
        DO 71 M=2,36
        K2=M-1
        DO 70 N=1,K2
        DELL=ABS(EL(M)-EL(N))
        DELG=ABS(G(M)-G(N))
9       IF(DELL .NE. 1.)  GO TO 70
        IF (DELG .GT. 2.1) GO TO 70
        DEL=ENN(M)*(G(N)+1.)-ENN(N)*(G(M)+1.)
        IF(DEL .LT. 0.0) GO TO 70
        FREQ=(E(M)-E(N))
        WVLTH = 1. /(FREQ)
        POWER = (FREQ)*R(M,N)
        GAIN= (2.93E-22)*DEL*R(M,N)/((FREQ)**3*(G(N)+1.))
        WRITE (6,80) M,N,DEL,FREQ,GAIN,POWER,WVLTH
   80   FORMAT (14,I3,E15.3,F15.7,E15.3,E15.3,E20.6)
   70   CONTINUE
   71   CONTINUE
        STOP
        END
```

```
63643334272     1       201466343466    2       202413412172    3       202414631463
41615440176     6       224750220000    7       151655376246    10      266434157115

MS
```

Section 7. The matrix A^{-1} is formed by the method of partial pivoting (Subrouting INVE, U.W.O. Dept. of Computer Science).

Section 8. Relative level populations are calculated using equation (V-8) with the assumption:

$R(m) = 1$ for $m = 30\text{-}36$

$R(m) = 0$ for $m \neq 30\text{-}36$

made as an approximation to the resonance character of the charge-transfer excitation cross section.

Section 9. Taking proper account of the degeneracy factors, and assuming doppler-broadened lines at a temperature $T_{gas} \sim 600^{\circ}K$, the negative absorption coefficients (GAIN) and the relative radiative powers are calculated for transitions between inverted levels using eq.(V-9) (multiplied by ω) and eq.(V-10). Here, the gains have been normalized to correspond to an excitation rate, R(m=30-36) = 10^{16} cm^{-3} sec^{-1} which would be expected to apply under discharge conditions similar to that of existing metal vapor - rare gas lasers, assuming an excitation cross section

on the order of $5 \cdot 10^{-15}$ cm^2.

V-3: Results and Discussion

The results of the machine calculations are presented on pages 83 and 84. We have indicated by brackets on the print-out and by transition arrows on the energy level diagram those transition groups (excepting the 96 micron lines, to be explained below) which have a gain greater than 1% per meter and are therefore of practical interest for application to lasing.

All but two wavelengths are in the infrared portion of the spectrum. The visible lines are at 5402A and 6821A, and have gains of roughly 2% per meter. The 5402A line is seen to have the highest power among inverted transitions. Several of the infrared lines are seen to have quite large gains, the largest being over 300% per meter for the 4.1 and 4.5 lines.

We wish to draw attention now to two important points regarding the above results. The first point concerns our neglect of collisional excitation and de-excitation processes among the levels resulting from gas-kinetic collisions. This can be shown to be justifiable for transitions which involve energy changes substantially greater

M	N	DEL	FORCE	GAIN	POWER	WEALTH
7	4	0.1838E+09	0.1081561	0.746E-03	0.381E+07	0.9245906+01
7	6	0.449E+09	0.0912948	0.711E-03	0.150E+07	0.1095356+02
8	4	0.270E+09	0.1084611	0.110E-02	0.386E+07	0.9219906+01
8	5	0.110E+10	0.0916089	0.104E-02	0.137E+07	0.1091606+02
8	6	0.705E+09	0.0915998	0.111E-03	0.151E+06	0.1091716+02
14	1	0.134E+09	0.2764971	0.211E-07	0.616E+04	0.3616676+01
14	6	0.351E+09	0.2596358	0.424E-05	0.750E+06	0.3851556+01
14	9	0.136E+09	0.0466070	0.166E-02	0.402E+06	0.2141926+02
14	10	0.276E+09	0.0414210	0.158E-02	0.269E+06	0.2413036+02
15	4	0.228E+09	0.2766381	0.352E-07	0.618E+04	0.3614936+01
15	5	0.971E+09	0.2597859	0.705E-05	0.677E+06	0.3849326+01
15	6	0.621E+09	0.2597768	0.744E-06	0.745E+05	0.3849466+01
15	9	0.232E+09	0.0468280	0.207E-02	0.407E+06	0.2135476+02
15	10	0.391E+09	0.0415691	0.259E-03	0.270E+05	0.2405646+02
15	11	0.691E+09	0.0415691	0.278E-02	0.246E+06	0.2405646+02
17	12	0.971E+08	0.0962110	0.781E-05	0.141E+06	0.1039386+02
18	12	0.754E+08	0.0962110	0.290E-06	0.675E+04	0.1039386+02
18	13	0.156E+09	0.0962110	0.881E-05	0.133E+06	0.1039386+02
21	4	0.172E+09	0.3581791	0.698E-08	0.456E+04	0.2791906+01
21	6	0.427E+09	0.3413178	0.968E-09	0.420E+03	0.2929026+01
21	9	0.174E+09	0.1283690	0.706E-06	0.752E+04	0.7790046+01
21	10	0.312E+09	0.1231100	0.150E-04	0.151E+06	0.8122926+01
21	16	0.227E+09	0.0242500	0.650E-02	0.675E+05	0.4124716+02
21	17	0.415E+09	0.0220200	0.776E-02	0.600E+05	0.4541336+02
22	WQ	0.309E+09	0.3582551	0.125E-07	0.456E+04	0.2791316+01
22	5	0.121E+10	0.3414029	0.165E-08	0.379E+03	0.2929096+01
22	6	0.783E+09	0.1283958	0.176E-09	0.417E+02	0.2929176+01
22	9	0.313E+09	0.1284450	0.127E-05	0.754E+04	0.7785436+01
22	10	0.553E+09	0.1231850	0.264E-05	0.150E+05	0.8117816+01
22	11	0.935E+09	0.1231850	0.270E-04	0.136E+06	0.8117816+01
22	16	0.419E+09	0.0243250	0.120E-01	0.684E+05	0.4110836+02
22	17	0.760E+09	0.0220950	0.141E-02	0.603E+04	0.4525716+02
22	18	0.119E+10	0.0220950	0.133E-01	0.548E+05	0.4525716+02
24	12	0.667E+08	0.1510030	0.483E-06	0.771E+05	0.6622126+01
24	19	0.170E+09	0.0521070	0.559E-04	0.496E+05	0.1919136+02
25	12	0.302E+08	0.1510070	0.105E-07	0.366E+04	0.6622126+01
25	13	0.944E+08	0.1510090	0.484E-06	0.728E+05	0.6622126+01
25	19	0.185E+09	0.0521070	0.291E-05	0.237E+04	0.1919136+02
25	20	0.262E+09	0.0521070	0.610E-04	0.468E+05	0.1919136+02
30	2	0.797E+09	0.7646038	0.900E-09	0.263E+04	0.1307876+01
30	3	0.167E+10	0.7636833	0.189E-08	0.526E+04	0.1309436+01
30	7	0.750E+09	0.3150900	0.110E-04	0.989E+06	0.3173706+01

M	N	DEL	FREQ	GAIN	POWER	WVLTH
30	8	0.160E+10	0.3147850	0.235E-04	0.197E+07	0.317677E+01
30	14	0.799E+09	0.1467490	0.750E-04	0.297E+06	0.681436E+01
30	15	0.164E+10	0.1466080	0.154E-03	0.593E+06	0.682091E+01
30	21	0.761E+09	0.0650670	0.587E-03	0.945E+05	0.153688E+02
30	22	0.156E+10	0.0649910	0.120E-02	0.188E+06	0.153867E+02
31	12	0.600E+08	0.1839800	0.278E-06	0.109E+06	0.543537E+01
31	19	0.163E+09	0.0850780	0.610E-05	0.402E+05	0.117539E+02
31	26	0.154E+09	0.0313540	0.139E-03	0.179E+05	0.318938E+02
32	13	0.391E+08	0.1839800	0.128E-06	0.103E+06	0.543537E+01
32	19	0.144E+09	0.0850780	0.257E-06	0.192E+04	0.117539E+02
32	20	0.207E+09	0.0850780	0.548E-05	0.379E+05	0.117539E+02
32	26	0.130E+09	0.0313540	0.562E-05	0.854E+03	0.318938E+02
32	27	0.192E+09	0.0313540	0.123E-03	0.169E+05	0.318938E+02
33	5	0.114E+10	0.4081139	0.112E-05	0.554E+06	0.245080E+01
33	6	0.723E+09	0.4081048	0.148E-04	0.774E+07	0.245035E+01
33	10	0.376E+09	0.1898970	0.461E-04	0.217E+07	0.526601E+01
33	11	0.724E+09	0.1898970	0.422E-05	0.155E+06	0.526601E+01
33	17	0.688E+09	0.0888070	0.451E-03	0.557E+06	0.112604E+02
33	18	0.110E+10	0.0888070	0.345E-04	0.399E+05	0.112604E+02
33	24	0.718E+09	0.0340090	0.458E-02	0.116E+06	0.294040E+02
33	25	0.115E+10	0.0340090	0.349E-03	0.835E+04	0.294040E+02
33	28	0.185E+10	0.0322860	0.370E-03	0.594E+04	0.309732E+02
33	31	0.725E+09	0.0010380	0.462E-01	0.101E+01	0.963391E+03
33	32	0.119E+10	0.0010380	0.362E-02	0.723E-01	0.963391E+03
34	5	0.107E+10	0.4081139	0.155E-04	0.822E+07	0.245030E+01
34	11	0.513E+09	0.1898970	0.444E-04	0.230E+07	0.526601E+01
34	18	0.102E+10	0.0868070	0.473E-03	0.592E+06	0.112604E+02
34	25	0.108E+10	0.0340090	0.487E-02	0.124E+06	0.294040E+02
34	28	0.187E+10	0.0322860	0.101E+04	0.160E+03	0.309732E+02
34	29	0.234E+10	0.0322860	0.363E-03	0.576E+04	0.309732E+02
34	32	0.113E+10	0.0010380	0.511E-01	0.107E+01	0.963391E+03
35	12	0.890E+09	0.1851020	0.269E-03	0.725E+07	0.540243E+01
35	13	0.126E+10	0.1851020	0.102E-04	0.261E+06	0.540243E+01
35	19	0.110E+10	0.0862000	0.494E-03	0.509E+06	0.116009E+02
35	20	0.148E+10	0.0862000	0.180E-04	0.183E+05	0.116009E+02
35	26	0.108E+10	0.0324760	0.643E-02	0.136E+06	0.307920E+02
35	27	0.146E+10	0.0324760	0.235E-03	0.488E+04	0.307920E+02
36	13	0.119E+10	0.1851020	0.277E-03	0.750E+07	0.540243E+01
36	20	0.148E+10	0.0862000	0.512E-03	0.527E+06	0.116089E+02
36	27	0.144E+10	0.0324760	0.665E-02	0.140E+06	0.307920E+02

EXIT
*C

metastable level) and is thus evidently a characteristic of hydrogenic wavefunctions.

CHAPTER VI

CONCLUSIONS

On the basis of what we have learned of the excitation processes in the cathode region of a glow discharge through metal vapor - rare gas mixtures, it is now possible to form some general conclusions regarding the suitability of this region for exciting laser action in these systems.

One of the most important and definite conclusions one can make concerns the limitation imposed on the relative metal vapor concentration. We have shown that quenching of the excitation of the upper laser levels with increasing metal vapor concentration does occur in the cathode region and at a relative concentration close to that of the positive column. This imposes an important requirement for optimizing the output from metal vapor - rare gas lasers operating in the cathode region--namely, the metal vapor concentration and discharge current must be independently controllable. The recently developed hollow cathode lasers which derive the metal vapor through sputtering or discharge heating do <u>not</u> satisfy this requirement.

context of the model presented in Section III.4-2, the ion drift velocity will begin to increase linearly with the distance from the negative glow while the concentration of rare gas metastables will fall exponentially (indicated by the lower dotted profile in region II and III of Figure III-7). Thus, an increase in the maximum output power density relative to that of the positive column may be available in a region adjacent to the negative glow and of width $\sim \alpha^{-\prime} = (D_m \tau_m)$ where D_m and τ_m are now the diffusion coefficient and lifetime of the rare gas metastables. The resulting net increase in power will depend on the width, $\alpha^{-\prime}$, of the layer and on the average field within the layer.

Now consider the behavior of a laser line excited by charge-transfer. If $\alpha^{-\prime}$ for the excitation carrier ion is small relative to the width of regions II and III in Figure III-7, then the behavior will follow from the same argument presented above for Penning excitation. On the other hand, if a significant fraction of the excitation carrier ions reach region IV before being converted to metal vapor ions, then the original model proposed for achieving laser action in the Crookes dark space becomes applicable, excepting the calculation of optimal metal vapor concentration. The

quenching action will limit the metal vapor concentration to roughly 1/10 of that calculated from the mean free path argument (eq.III-10). This brings the estimate of output enhancement relative to the positive column down to below one order of magnitude. In this case, cathode-fall voltages in the kilo-volt range and the use of short pulses to limit discharge heating and arcing will be required.

The above conclusions are valid only within the context of the simplified model presented in Section III.4-2 and depend sensitively on the parameter α . The buffer zone will obviously play an important role in a more complete model, and this points to the need for measuring the electric field profiles within this zone simultaneously with the emission profiles. Valuable information regarding the parameter α could also be gained from a careful study of the response of the anomalous profiles to an order of magnitude reduction of the metal vapor concentration. This requires much more sophisticated optics than were used in the profile measurements of Chapter III.

In addition to the conclusions already drawn at the end of Chapter IV regarding possible applications of the grid enhancement effect, we can mention here, modulation, as yet another important possible application. The grid circuit

was shown to draw only a small fraction of the power drawn by the discharge itself, and although it will be limited to low speeds, it seems uniquely suited for such an application.

It is felt that the discovery of the enhancement effect of the grid will be of major importance in the future development of cathode region lasers.

Finally, we have developed in Chapter V a computer program which has predicted inversions on transitions in MgII resulting from the reaction:

$$Ne^{+} + Mg \rightarrow (Mg^{+})^{*} + Ne$$

and cascade processes. Future work is planned which will apply the calculations to other systems and incorporate into the program calculations of the charge-transfer cross sections using techniques developed by Smith.[23]

REFERENCES

1. J. W. McGowan and R. F. Stebbings, Applied Optics Supplement, 2, 68 (1965).

2. L. I. Gudzenko and L. A. Shelpin, J.E.T.P. Letters, 7, 190 (1968).

3. B. M. Smirnov, J.E.T.P. Letters, 6, 78 (1967).

4. R. C. Jensen and W. R. Bennett, Jr., IEEE J. Quantum Electronics QE-4, 356 (1968).

5. R. C. Jensen and G. J. Collins, and W. R. Bennett, Jr., Phys. Rev. Letters, 23, 363 (1969).

6. G. J. Collins, Ph.D. Thesis, Yale University, 1970.

7. W. T. Silvfast, G. R. Fowles, and B. D. Hopkins, Applied Physics Letters, 8, 318 (1966).

8. S. Flugge, Handbuch Der Physik (Springer-Verlag, Berlin, 1956), p. 186.

9. Y. Sugawara and Y. Tokiwa, Japanese J. of Applied Physics, 9, 588 (1970).

10. W. K. Schuebel, Applied Phys. Letters, 16, 470 (1970).

11. W. K. Schuebel, IEEE J. Quantum Electronics, QE-6, 574 (1970).

12. A. J. Palmer, J. of Applied Physics, 41, 3906 (1970).

13. A. von Engel, Ionized Gases (Oxford University Press, 1965).

14. S. C. Brown, Basic Data of Plasma Physics (The M.I.T. Press, Cambridge, Massachusetts, 1959).

15. L. B. Loeb, Basic Processes of Gaseous Electronics (University of California Press, Berkeley, 1961).

16. D. H. Pringle and W. E. J. Farvis, Proc. Phys. Soc. 68, 836 (1955).

17. W. C. Holton and L. D. Shearer, 6th International Quantum Electronics Conference, Kyoto (1970).

18. H. S. W. Massey and E. H. S. Burhop, Electronic and Ionic Impact Phenomena (Clarendon Press, Oxford, 1952), p. 441.

19. D. R. Bates and A. Damgaard, Phil. Trans. Roy. Soc. London, Ser. A, 242, 101 (1949).

20. J. H. Manley and O. S. Duffendack, Phys. Rev. 47, 56 (1935).

21. H. R. Griem, Plasma Spectroscopy (McGraw-Hill, New York, 1964).

22. H. A. Bethe and E. E. Salpeter, Quantum Mechanics of One and Two Electron Atoms (Academic Press Inc., New York, 1957), p. 266.

23. F. T. Smith and R. E. Olson, 23rd Annual Gaseous Electronics Conference, Hartford (1970).